

A SYMMETRIZED PARAMETRIC FINITE ELEMENT METHOD FOR ANISOTROPIC SURFACE DIFFUSION OF CLOSED CURVES*

WEIZHU BAO[†], WEI JIANG[‡], AND YIFEI LI[†]

Abstract. We deal with a long-standing problem about how to design an energy-stable numerical scheme for solving the motion of a closed curve under *anisotropic surface diffusion* with a general anisotropic surface energy $\gamma(\mathbf{n})$ in two dimensions, where \mathbf{n} is the outward unit normal vector. By introducing a novel surface energy matrix $\mathbf{Z}_k(\mathbf{n})$ which depends on the Cahn–Hoffman $\boldsymbol{\xi}$ -vector and a stabilizing function $k(\mathbf{n})$, we first reformulate the equation into a conservative form and derive a new symmetrized variational formulation for anisotropic surface diffusion with weakly or strongly anisotropic surface energies. Then, a semidiscretization in space for the variational formulation is proposed, and its area conservation and energy dissipation properties are proved. The semidiscretization is further discretized in time by an implicit structural-preserving scheme (SP-PFEM) which can rigorously preserve the enclosed area in the fully discrete level. Furthermore, we prove that the SP-PFEM is unconditionally energy-stable for almost any anisotropic surface energy $\gamma(\mathbf{n})$ under a simple and mild condition on $\gamma(\mathbf{n})$. For several commonly used anisotropic surface energies, we construct $\mathbf{Z}_k(\mathbf{n})$ explicitly. Finally, extensive numerical results are reported to demonstrate the high performance of the proposed scheme.

Key words. anisotropic surface diffusion, Cahn–Hoffman $\boldsymbol{\xi}$ -vector, anisotropic surface energy, parametric finite element method, structure-preserving, energy-stable, surface energy matrix

MSC codes. 65M60, 65M12, 35K55, 53C44

DOI. 10.1137/22M1472851

1. Introduction. Anisotropic surface diffusion is an important and common process at material surfaces/interfaces in solids due to different surface lattice orientations. The lattice orientational difference leads to anisotropic surface energy in solid materials. It thus generates an anisotropic evolution process for a solid material. Recently, anisotropic surface diffusion has been regarded as an important kinetic process in surface phase formation, epitaxial growth, heterogeneous catalysis, and many other areas in surface/materials science [34]. It has seen significant and broader applications in materials science, computational geometry, and solid-state physics, such as the evolution of voids in microelectronic circuits [30, 43], microstructure evolution in solids [11, 17], the smoothing of discrete surfaces [13], and solid-state dewetting [37, 45, 22, 39].

As shown in Figure 1.1, for a closed curve Γ in two dimensions associated with a given anisotropic surface energy $\gamma(\mathbf{n})$, where $\mathbf{n} = (n_1, n_2)^T \in \mathbb{S}^1$ representing the

*Received by the editors January 20, 2022; accepted for publication (in revised form) October 24, 2022; published electronically March 28, 2023.

<https://doi.org/10.1137/22M1472851>

Funding: The work of the first author was supported by the Ministry of Education of Singapore, grant MOE2019-T2-1-063 (R-146-000-296-112). The work of the second author was supported by the National Natural Science Foundation of China, grants 12271414 and 11871384, and the National Key Research and Development Program of China, grant 2020YFA0714201.

[†]Department of Mathematics, National University of Singapore, Singapore, 119076 (matbaowz@nus.edu.sg, e0444158@u.nus.edu).

[‡]School of Mathematics and Statistics, and Hubei Key Laboratory of Computational Science, Wuhan University, Wuhan, 430072, People’s Republic of China (jiangwei1007@whu.edu.cn).

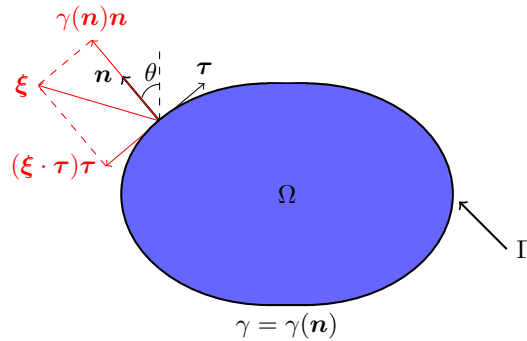


FIG. 1.1. An illustration of a closed curve Γ in \mathbb{R}^2 under anisotropic surface diffusion with an anisotropic surface energy $\gamma(\mathbf{n})$, where \mathbf{n} is the outward unit normal vector, $\boldsymbol{\tau}$ is the unit tangential vector, $\boldsymbol{\xi}$ is the Cahn–Hoffman vector in (1.3), and θ is the angle between \mathbf{n} and the y -axis such that $\mathbf{n} = (-\sin \theta, \cos \theta)^T$ with $\theta \in [-\pi, \pi]$.

unit outward normal vector, the motion by anisotropic surface diffusion of the curve is described by the geometric evolution equation [32, 12]

$$(1.1) \quad V_n = \partial_{ss}\mu,$$

where V_n is the normal velocity, s is the arclength parameter of Γ , and $\mu := \mu(s)$ is the chemical potential (or weighted curvature denoted as $\kappa_\gamma := \kappa_\gamma(s)$ in the literature [35]) generated from the energy functional $W(\Gamma) := \int_\Gamma \gamma(\mathbf{n}) ds$ via the thermodynamic variation [12, 3]. It is well-known that the anisotropic surface diffusion has the following two essential geometric properties: (i) the area of the region enclosed by the curve is conserved, and (ii) the free energy (or weighted length) $W(\Gamma)$ of the curve decreases in time [39, 3, 27]. More precisely, the motion by anisotropic surface diffusion is the H^{-1} -gradient flow of the free energy (or weighted length) functional $W(\Gamma)$ [36, 31].

Let $\gamma(\mathbf{p}) : \mathbb{R}^2 \rightarrow \mathbb{R}$ be a homogeneous extension of the anisotropic surface energy $\gamma(\mathbf{n}) : \mathbb{S}^1 \rightarrow \mathbb{R}^+$ satisfying (i) $\gamma(\mathbf{p})|_{\mathbf{p}=\mathbf{n}} = \gamma(\mathbf{n})$ for $\mathbf{n} \in \mathbb{S}^1$, and (ii) $\gamma(c\mathbf{p}) = c\gamma(\mathbf{p})$ for $c > 0$ and $\mathbf{p} \in \mathbb{R}^2$. A typical homogeneous extension is widely used in the literature as [25, 14]

$$(1.2) \quad \gamma(\mathbf{p}) := \begin{cases} |\mathbf{p}| \gamma\left(\frac{\mathbf{p}}{|\mathbf{p}|}\right) & \forall \mathbf{p} = (p_1, p_2)^T \in \mathbb{R}_*^2 := \mathbb{R}^2 \setminus \{\mathbf{0}\}, \\ 0, & \mathbf{p} = \mathbf{0}, \end{cases}$$

where $|\mathbf{p}| = \sqrt{p_1^2 + p_2^2}$. Then the Cahn–Hoffman $\boldsymbol{\xi}$ -vector introduced by Cahn and Hoffman is mathematically given by [20, 40]

$$(1.3) \quad \boldsymbol{\xi} := \boldsymbol{\xi}(\mathbf{n}) = \nabla \gamma(\mathbf{p})|_{\mathbf{p}=\mathbf{n}} = \gamma(\mathbf{n})\mathbf{n} + (\boldsymbol{\xi} \cdot \boldsymbol{\tau})\boldsymbol{\tau} \quad \forall \mathbf{n} \in \mathbb{S}^1,$$

where $\boldsymbol{\tau} = \mathbf{n}^\perp$ is the unit tangential vector with the notation $^\perp$ denoting clockwise rotation by $\frac{\pi}{2}$ (cf. Figure 1.1). Furthermore, the chemical potential μ (or weighted curvature) and the Hessian matrix $\mathbf{H}_\gamma(\mathbf{n})$ are defined as [25]

$$(1.4) \quad \mu := -\mathbf{n} \cdot \partial_s \boldsymbol{\xi}^\perp, \quad \mathbf{H}_\gamma(\mathbf{n}) := \nabla \nabla \gamma(\mathbf{p})|_{\mathbf{p}=\mathbf{n}}, \quad \forall \mathbf{n} \in \mathbb{S}^1.$$

We remark here that $\mathbf{H}_\gamma(\mathbf{n})\mathbf{n} = \mathbf{0}$ and thus 0 is an eigenvalue of $\mathbf{H}_\gamma(\mathbf{n})$ and \mathbf{n} is a corresponding eigenvector. We denote the other eigenvalue of $\mathbf{H}_\gamma(\mathbf{n})$ as $\lambda(\mathbf{n}) \in \mathbb{R}$.

The Frank diagram \mathcal{F} of $\gamma(\mathbf{n})$ is defined as $\mathcal{F} := \{\mathbf{p} \in \mathbb{R}^2 \mid \gamma(\mathbf{p}) \leq 1\}$, i.e., $1/\gamma$ plot (see page 190 in [14]).

Let $\Gamma := \Gamma(t)$ be parameterized by $\mathbf{X} := \mathbf{X}(s, t) = (x(s, t), y(s, t))^T \in \mathbb{R}^2$ with t representing the time and s denoting the arclength parametrization of Γ (cf. Figure 1.1); then via the Cahn–Hoffman $\boldsymbol{\xi}$ -vector in (1.3), the anisotropic surface diffusion equation (1.1) for Γ is described as follows [25]:

$$(1.5a) \quad \partial_t \mathbf{X} = \partial_{ss} \mu \mathbf{n}, \quad 0 < s < L(t), \quad t > 0,$$

$$(1.5b) \quad \mu = -\mathbf{n} \cdot \partial_s \boldsymbol{\xi}^\perp, \quad \boldsymbol{\xi} = \nabla \gamma(\mathbf{p})|_{\mathbf{p}=\mathbf{n}},$$

where $L(t) = \int_{\Gamma(t)} ds$ is the length of $\Gamma(t)$, and

$$(1.6) \quad \boldsymbol{\tau} = \partial_s \mathbf{X} = \mathbf{n}^\perp, \quad \mathbf{n} = -\partial_s \mathbf{X}^\perp = -\boldsymbol{\tau}^\perp.$$

The initial data for (1.5) is given as

$$(1.7) \quad \mathbf{X}(s, 0) = \mathbf{X}_0(s) = (x_0(s), y_0(s))^T, \quad 0 \leq s \leq L_0,$$

where L_0 represents the length of the initial curve $\Gamma_0 = \Gamma(0)$.

When $\gamma(\mathbf{n}) \equiv 1$, it is called *isotropic* surface energy; in the isotropic case, $\gamma(\mathbf{p}) = |\mathbf{p}|$ in (1.2), $\boldsymbol{\xi} = \mathbf{n}$ in (1.3), and $\mu = \kappa$ and $\mathbf{H}_\gamma(\mathbf{n}) \equiv I_2 - \mathbf{n}\mathbf{n}^T$ in (1.4) with κ the curvature and I_2 the 2×2 identity matrix and $\lambda(\mathbf{n}) \equiv 1$, and thus (1.5) collapses to the (isotropic) surface diffusion [6, 32, 26, 47]. In contrast, when $\gamma(\mathbf{n})$ is not a constant, it is called *anisotropic* surface energy, and in the anisotropic case, when $\boldsymbol{\tau}^T \mathbf{H}_\gamma(\mathbf{n}) \boldsymbol{\tau} \geq 0$ for all $\mathbf{n} \in \mathbb{S}^1$ with $\boldsymbol{\tau} = \mathbf{n}^\perp$ ($\Leftrightarrow \lambda(\mathbf{n}) \geq 0$ for $\mathbf{n} \in \mathbb{S}^1 \Leftrightarrow \tilde{\gamma}(\theta) := \hat{\gamma}(\theta) + \hat{\gamma}''(\theta) \geq 0$ for all $\theta \in [-\pi, \pi]$ with $\hat{\gamma}(\theta) := \gamma(\mathbf{n}) = \gamma(-\sin \theta, \cos \theta) \Leftrightarrow$ the Frank diagram of $\gamma(\mathbf{n})$ is convex), it is called *weakly anisotropic*; otherwise, when $\boldsymbol{\tau}^T \mathbf{H}_\gamma(\mathbf{n}) \boldsymbol{\tau}$ changes sign for $\mathbf{n} \in \mathbb{S}^1$ ($\Leftrightarrow \lambda(\mathbf{n})$ changes sign for $\mathbf{n} \in \mathbb{S}^1 \Leftrightarrow \tilde{\gamma}(\theta)$ changes sign for $\theta \in [-\pi, \pi] \Leftrightarrow$ the Frank diagram of $\gamma(\mathbf{n})$ is not convex), it is called *strongly anisotropic*.

Some commonly used anisotropic surface energies $\gamma(\mathbf{n})$ are summarized below:

(i) the Riemannian-like metric (also called BGN) anisotropic surface energy [7, 10]

$$(1.8) \quad \gamma(\mathbf{n}) = \sum_{l=1}^L \gamma_l(\mathbf{n}) = \sum_{l=1}^L \sqrt{\mathbf{n}^T \mathbf{G}_l \mathbf{n}} \quad \forall \mathbf{n} \in \mathbb{S}^1,$$

where $\mathbf{G}_l \in \mathbb{R}^{2 \times 2}, l = 1, \dots, L$, are symmetric and positive definite matrices;

(ii) the l^r -norm metric anisotropic surface energy [14]

$$(1.9) \quad \gamma(\mathbf{n}) = \|\mathbf{n}\|_{l^r} = (|n_1|^r + |n_2|^r)^{\frac{1}{r}} \quad \forall \mathbf{n} = (n_1, n_2)^T \in \mathbb{S}^1,$$

where $1 < r < \infty$;

(iii) the m -fold anisotropic surface energy [4]

$$(1.10) \quad \gamma(\mathbf{n}) = 1 + \beta \cos(m(\theta - \theta_0)) \quad \forall \mathbf{n} = (n_1, n_2)^T = (-\sin \theta, \cos \theta)^T \in \mathbb{S}^1,$$

where $m = 2, 3, 4, 6$, $\theta_0 \in [0, \pi]$ is a phase shift angle, and $\beta \geq 0$ controls the degree of the anisotropy;

(iv) the regularized l^1 -norm metric anisotropic surface energy which can be viewed as a regularization for the nonsmooth surface energy $\gamma(\mathbf{n}) = |n_1| + |n_2|$ [7, 9]

$$(1.11) \quad \gamma(\mathbf{n}) = \sqrt{n_1^2 + \varepsilon^2 n_2^2} + \sqrt{\varepsilon^2 n_1^2 + n_2^2} \quad \forall \mathbf{n} = (n_1, n_2)^T \in \mathbb{S}^1,$$

where $0 < \varepsilon \ll 1$ is a small “artificial” regularization parameter. This regularization can be treated as a special case of (1.8).

For the convenience of readers, we list $\gamma(\mathbf{p})$, $\boldsymbol{\xi}(\mathbf{n})$, $\lambda(\mathbf{n})$, and $\mathbf{H}_\gamma(\mathbf{n})$ of the above surface energies in Appendix A.

Different numerical methods have been proposed for the isotropic/anisotropic surface diffusion, such as the marker-particle method [41, 16], the finite element method via graph representation [1, 14, 15], the θ - L formulation method [21], the discontinuous Galerkin finite element method [44], and the parametric finite element method (PFEM) [6, 8, 19, 4, 25, 29]. Among these methods, the PFEM performs the best in terms of accuracy and efficiency as well as mesh quality in practical computations via reformulating (1.5) as [25]

$$(1.12a) \quad \mathbf{n} \cdot \partial_t \mathbf{X} = \partial_{ss} \mu, \quad 0 < s < L(t), \quad t > 0,$$

$$(1.12b) \quad \mu \mathbf{n} = -\partial_s \boldsymbol{\xi}^\perp, \quad \boldsymbol{\xi} = \nabla \gamma(\mathbf{p})|_{\mathbf{p}=\mathbf{n}}.$$

When $\gamma(\mathbf{n}) \equiv 1$ (i.e., isotropic surface energy), noting $\mu = \kappa$ and $\mathbf{n} = -\partial_s \mathbf{X}^\perp$, then (1.12b) collapses to $\kappa \mathbf{n} = -\partial_{ss} \mathbf{X}$. In this case, the PFEM is semi-implicit, is unconditionally energy-stable, and enjoys asymptotic equal mesh distribution [6], and thus there is no need to remesh during time evolution. Very recently, a structure-preserving PFEM (SP-PFEM) was proposed for the surface diffusion [5, 2]. However, when the PFEM is extended directly to simulate anisotropic surface diffusion, many good properties are no longer preserved, especially for the unconditional energy stability, which can be preserved only for a very special Riemannian-like metric anisotropic surface energy in (1.8) with a modified variational formulation [7]. Recently, by reformulating (1.12b) into a conservative form, an energy-stable PFEM was designed for weakly anisotropic surface diffusion under a very strong condition on $\hat{\gamma}(\theta) = \gamma(-\sin \theta, \cos \theta)$ [29]. To our best knowledge, it is still an open question to design an unconditionally energy-stable scheme for solving the anisotropic surface diffusion (1.12) with any form of $\gamma(\mathbf{n})$.

The objective of this paper is to propose an unconditionally energy-stable SP-PFEM for solving the anisotropic surface diffusion (1.12) with the surface energy $\gamma(\mathbf{n})$ satisfying a relatively mild condition as

$$(1.13) \quad \gamma(-\mathbf{n}) = \gamma(\mathbf{n}) \quad \forall \mathbf{n} \in \mathbb{S}^1, \quad \gamma(\mathbf{p}) \in C^2(\mathbb{R}^2 \setminus \{\mathbf{0}\}).$$

We first reformulate (1.12b) into a conservative and self-adjoint form by introducing a novel symmetric positive definite surface energy matrix $\mathbf{Z}_k(\mathbf{n})$ depending on the Cahn–Hoffman $\boldsymbol{\xi}$ -vector and a stabilizing function $k(\mathbf{n})$, and then we derive a new symmetrized variational formulation for the anisotropic surface diffusion (1.12). The symmetrized variational formulation is first discretized in space by PFEM and then discretized in time by an implicit SP-PFEM which preserves the area in the fully discrete level. Under the simple and mild condition (1.13) on $\gamma(\mathbf{n})$, we rigorously prove that the SP-PFEM is energy dissipative and thus is unconditionally energy-stable for almost all anisotropic surface energy $\gamma(\mathbf{n})$ arising in practical applications, including both weakly and strongly anisotropic surface energies.

The remainder of this paper is structured as follows. In section 2, we first introduce the surface energy matrix $\mathbf{Z}_k(\mathbf{n})$, propose a new symmetrized variational formulation, and show its area conservation and energy dissipation. In section 3, we present a semidiscretization in space by PFEM and a full discretization by an implicit SP-PFEM for the weak formulation. In section 4, we prove the unconditional energy-stability of SP-PFEM under the condition (1.13) on $\gamma(\mathbf{n})$. In section 5, numerical

results are given to demonstrate the high performance of the proposed SP-PFEM. Finally, we draw some conclusions in section 6.

2. A new symmetrized variational formulation and its properties. In this section, we present a new conservative and self-adjoint formulation of (1.12b) and a new symmetrized variational formulation of (1.12) and prove the area conservation and energy dissipation of the new formulation.

2.1. A symmetric positive definite surface energy matrix. Introducing a symmetric surface energy matrix $\mathbf{Z}_k(\mathbf{n})$ as

$$(2.1) \quad \mathbf{Z}_k(\mathbf{n}) = \gamma(\mathbf{n})I_2 - \mathbf{n}\boldsymbol{\xi}(\mathbf{n})^T - \boldsymbol{\xi}(\mathbf{n})\mathbf{n}^T + k(\mathbf{n})\mathbf{n}\mathbf{n}^T \quad \forall \mathbf{n} \in \mathbb{S}^1,$$

where $k(\mathbf{n}) : \mathbb{S}^1 \rightarrow \mathbb{R}^+$ is a stabilizing function to be determined later, then we have the following lemma.

LEMMA 2.1 (symmetric and conservative form). *With the symmetric surface energy matrix $\mathbf{Z}_k(\mathbf{n})$ in (2.1), the anisotropic surface diffusion (1.12b) can be reformulated as*

$$(2.2a) \quad \mathbf{n} \cdot \partial_t \mathbf{X} = \partial_{ss} \mu,$$

$$(2.2b) \quad \mu \mathbf{n} = -\partial_s (\mathbf{Z}_k(\mathbf{n}) \partial_s \mathbf{X}).$$

Proof. From (1.3), noting (1.6), we get

$$(2.3) \quad \boldsymbol{\xi}^\perp = \gamma(\mathbf{n})\mathbf{n}^\perp + (\boldsymbol{\xi} \cdot \boldsymbol{\tau})\boldsymbol{\tau}^\perp = \gamma(\mathbf{n})\boldsymbol{\tau} - (\boldsymbol{\xi} \cdot \boldsymbol{\tau})\mathbf{n}.$$

From (2.1), noticing (1.6) and (2.3), and using $\mathbf{n} \cdot \boldsymbol{\tau} = 0$, we get

$$(2.4) \quad \begin{aligned} \mathbf{Z}_k(\mathbf{n})\partial_s \mathbf{X} &= \mathbf{Z}_k(\mathbf{n})\boldsymbol{\tau} = (\gamma(\mathbf{n})I_2 - \mathbf{n}\boldsymbol{\xi}^T - \boldsymbol{\xi}\mathbf{n}^T + k(\mathbf{n})\mathbf{n}\mathbf{n}^T)\boldsymbol{\tau} \\ &= \gamma(\mathbf{n})\boldsymbol{\tau} - (\boldsymbol{\xi} \cdot \boldsymbol{\tau})\mathbf{n} + (\mathbf{n} \cdot \boldsymbol{\tau})(k(\mathbf{n})\mathbf{n} - \boldsymbol{\xi}) = \boldsymbol{\xi}^\perp. \end{aligned}$$

Plugging (2.4) into (1.12), we obtain (2.2) immediately. \square

Remark 2.1. When $\gamma(\mathbf{n}) \equiv 1$ and by taking $k(\mathbf{n}) \equiv 2$ in (2.1), we have $\mu = \kappa$ and $\boldsymbol{\xi} = \mathbf{n}$, and thus $\mathbf{Z}_k(\mathbf{n}) \equiv I_2$. Then (2.2) collapses to the standard formulation by PFEM for surface diffusion [6]. Similarly, when $\gamma(\mathbf{n})$ is chosen as the Riemannian-like metric anisotropic surface energy (1.8), by taking $k(\mathbf{n}) = \sum_{l=1}^L \gamma_l(\mathbf{n})^{-1} \text{Tr}(\mathbf{G}_l)$ with $\text{Tr}(\mathbf{G}_l)$ denoting the trace of \mathbf{G}_l , then (2.2) collapses to the formulation used in [7]. A similar formulation but without the symmetrizing term $-\boldsymbol{\xi}(\mathbf{n})\mathbf{n}^T$ and the stabilizing term $k(\mathbf{n})$ can also be found in [8, (1.18)].

2.2. The variational formulation. Let $\mathbb{T} = \mathbb{R}/\mathbb{Z} = [0, 1]$ be the periodic unit interval and we parameterize the evolution curves $\Gamma(t)$ as

$$(2.5) \quad \Gamma(t) := \mathbf{X}(\mathbb{T}, t), \quad \mathbf{X}(\rho, t) := (x(\rho, t), y(\rho, t))^T : \mathbb{T} \times \mathbb{R}^+ \rightarrow \mathbb{R}^2.$$

The arclength parameter s is computed by $s(\rho, t) = \int_0^\rho |\partial_q \mathbf{X}(q, t)| dq$ with its derivative $\partial_\rho s = |\partial_\rho \mathbf{X}|$. By the introduced time-independent variable ρ , the evolving curve $\Gamma(t)$ can then be parameterized over a fixed domain $\rho \in \mathbb{T} = [0, 1]$. We do not distinguish the two parameterizations $\mathbf{X}(\rho, t)$ and $\mathbf{X}(s, t)$ for $\Gamma(t)$ if there is no ambiguity. We also introduce the usual Sobolev space as

$$(2.6) \quad L^2(\mathbb{T}) = \left\{ u : \mathbb{T} \rightarrow \mathbb{R} \mid \int_{\mathbb{T}} |u(\rho)|^2 d\rho < +\infty \right\},$$

equipped with the weighted L^2 -inner product with respect to the closed curve $\Gamma(t)$

$$(2.7) \quad (u, v)_{\Gamma(t)} := \int_{\Gamma(t)} u(s)v(s)ds = \int_{\mathbb{T}} u(\rho)v(\rho)\partial_\rho s(\rho, t) d\rho \quad \forall u, v \in L^2(\mathbb{T}),$$

which can be easily extended to $[L^2(\mathbb{T})]^2$. Here, we always assume that $\partial_\rho s(\rho, t)$ is bounded for all t . Moreover, the Sobolev space $H^1(\mathbb{T})$ is given as

$$(2.8) \quad H^1(\mathbb{T}) := \{u : \mathbb{T} \rightarrow \mathbb{R}, \text{ and } u \in L^2(\mathbb{T}), \partial_\rho u \in L^2(\mathbb{T})\}.$$

Multiplying a test function $\varphi(\rho) \in H^1(\mathbb{T})$ to (2.2a), and then integrating over $\Gamma(t)$ and taking integration by parts, we have

$$(2.9) \quad (\mathbf{n} \cdot \partial_t \mathbf{X}, \varphi)_{\Gamma(t)} = (\partial_{ss}\mu, \varphi)_{\Gamma(t)} = -(\partial_s \mu, \partial_s \varphi)_{\Gamma(t)}.$$

Similarly, by multiplying a test function $\boldsymbol{\omega} = (\omega_1, \omega_2)^T \in [H^1(\mathbb{T})]^2$ to (2.2b), we obtain

$$(2.10) \quad (\boldsymbol{\mu} \mathbf{n}, \boldsymbol{\omega})_{\Gamma(t)} = (-\partial_s(\mathbf{Z}_k(\mathbf{n})\partial_s \mathbf{X}), \boldsymbol{\omega})_{\Gamma(t)} = (\mathbf{Z}_k(\mathbf{n})\partial_s \mathbf{X}, \partial_s \boldsymbol{\omega})_{\Gamma(t)}.$$

By combining the two weak formulations (2.9) and (2.10), we now get the novel symmetrized variational formulation for the anisotropic surface diffusion (2.2) (or (1.5)) with the initial condition (1.7). More precisely, for a given initial curve $\Gamma_0 := \Gamma(0) = \mathbf{X}(\mathbb{T}, 0)$ with $\mathbf{X}(\rho, 0) = \mathbf{X}_0(L_0\rho) \in [H^1(\mathbb{T})]^2$, find the solution $\Gamma(t) := \mathbf{X}(\mathbb{T}, t)$, $\mathbf{X}(\cdot, t) \in [H^1(\mathbb{T})]^2$ and $\mu(\cdot, t) \in H^1(\mathbb{T})$ such that

$$(2.11a) \quad (\mathbf{n} \cdot \partial_t \mathbf{X}, \varphi)_{\Gamma(t)} + (\partial_s \mu, \partial_s \varphi)_{\Gamma(t)} = 0 \quad \forall \varphi \in H^1(\mathbb{T}),$$

$$(2.11b) \quad (\boldsymbol{\mu}, \mathbf{n} \cdot \boldsymbol{\omega})_{\Gamma(t)} - (\mathbf{Z}_k(\mathbf{n})\partial_s \mathbf{X}, \partial_s \boldsymbol{\omega})_{\Gamma(t)} = 0 \quad \forall \boldsymbol{\omega} \in [H^1(\mathbb{T})]^2.$$

2.3. Area conservation and energy dissipation. Let $A(t)$ denote the area (i.e., the region $\Omega(t)$ enclosed by the curve $\Gamma(t)$) and let $W_c(t)$ denote the free energy (or weighted length), which are defined as

$$(2.12) \quad A(t) := \int_{\Omega(t)} 1 d\mathbf{x} = \int_0^{L(t)} y(s, t)\partial_s x(s, t) ds, \quad W_c(t) := \int_{\Gamma(t)} \gamma(\mathbf{n}) ds, \quad t \geq 0.$$

For the above variational problem (2.11), we have the following proposition.

PROPOSITION 2.2 (area conservation and energy dissipation). *The area $A(t)$ of the solution $(\mathbf{X}(\cdot, t), \mu(\cdot, t)) \in [H^1(\mathbb{T})]^2 \times H^1(\mathbb{T})$ defined by the variational problem (2.11) is conserved, and the energy $W_c(t)$ is dissipative, i.e.,*

$$(2.13) \quad A(t) \equiv \int_0^{L_0} y_0(s)x'_0(s)ds, \quad W_c(t) \leq W_c(t_1) \leq \int_0^{L_0} \gamma(\mathbf{n}) ds, \quad t \geq t_1 \geq 0.$$

Proof. The proof of area conservation is similar to the Proposition 2.1 in [29]; thus we omit the details for brevity.

To prove the energy dissipation in (2.13), taking the derivative of $W_c(t)$ with respect to t , noting (1.3), (2.4), (2.11b) with $\omega = \partial_t \mathbf{X}$, and (2.11a) with $\varphi = \mu$, and $\partial_t \mathbf{n} = (\boldsymbol{\tau} \cdot \partial_t \mathbf{n})\boldsymbol{\tau} = -(\mathbf{n} \cdot \partial_s \partial_t \mathbf{X})\boldsymbol{\tau}$, we have

$$\begin{aligned} \dot{W}_c(t) &= \frac{d}{dt} \int_0^{L(t)} \gamma(\mathbf{n}) ds = \frac{d}{dt} \int_0^1 \gamma(\mathbf{n}) \partial_\rho s d\rho = \int_0^1 (\gamma(\mathbf{n}) \partial_t \partial_\rho s + \nabla \gamma(\mathbf{n}) \cdot \partial_t \mathbf{n} \partial_\rho s) d\rho \\ &= \int_0^1 (\gamma(\mathbf{n})\boldsymbol{\tau} - (\boldsymbol{\xi} \cdot \boldsymbol{\tau})\mathbf{n}) \cdot \partial_s \partial_t \mathbf{X} \partial_\rho s d\rho = \left(\mathbf{Z}_k(\mathbf{n}) \partial_s \mathbf{X}, \partial_s \partial_t \mathbf{X} \right)_{\Gamma(t)} \\ &= - \left(\partial_s \mu, \partial_s \mu \right)_{\Gamma(t)} \leq 0, \end{aligned}$$

which implies the energy dissipation in (2.13). □

3. PFEM discretizations and their properties. In this section, we first discretize the variational problem (2.11) in space by PFEM and show its area conservation and energy dissipation. Then we further discretize the semidiscretization in time by an SP-PFEM which conserves area in the fully discrete level.

3.1. A semidiscretization in space by PFEM and its properties. Let $N > 0$ be an integer, the mesh size $h = 1/N$, the grid points $\rho_j = jh$ for $j = 0, 1, \dots, N$, and the subintervals $I_j = [\rho_{j-1}, \rho_j]$ for $j = 1, 2, \dots, N$. Then we can give a uniform partition of the torus \mathbb{T} by $\mathbb{T} = [0, 1] = \bigcup_{j=1}^N I_j$. Moreover, the finite element subspace of $H^1(\mathbb{T})$ is given by

$$\mathbb{K}^h = \mathbb{K}^h(\mathbb{T}) := \{u^h \in C(\mathbb{T}) \mid u^h|_{I_j} \in \mathcal{P}_1 \ \forall j = 1, 2, \dots, N\},$$

where \mathcal{P}_1 stands for the space of polynomials of degree at most 1.

Let the piecewise linear curve $\Gamma^h(t) := \mathbf{X}^h(\mathbb{T}, t)$, $\mathbf{X}^h(\cdot, t) = (x^h(\cdot, t), y^h(\cdot, t))^T \in [\mathbb{K}^h]^2$ be the numerical approximation of $\Gamma(t) := \mathbf{X}(\mathbb{T}, t)$, $\mathbf{X}(\cdot, t) \in [H^1(\mathbb{T})]^2$ and the piecewise linear function $\mu^h(\cdot, t) \in \mathbb{K}^h$ be the numerical approximation of $\mu(\cdot, t) \in H^1(\mathbb{T})$, where $(\mathbf{X}(\cdot, t), \mu(\cdot, t)) \in [H^1(\mathbb{T})]^2 \times H^1(\mathbb{T})$ is given by the variational problem (2.11). Then $\Gamma^h(t)$ is formed by ordered vectors $\{\mathbf{h}_j(t)\}_{j=1}^N$ and we assume that for $t \geq 0$, these vectors $\mathbf{h}_j(t)$ satisfy

$$(3.1) \quad h_{\min}(t) := \min_{1 \leq j \leq N} |\mathbf{h}_j(t)| > 0, \quad \mathbf{h}_j(t) := \mathbf{X}^h(\rho_j, t) - \mathbf{X}^h(\rho_{j-1}, t) \ \forall j,$$

where $|\mathbf{h}_j(t)|$ is the length of the vector $\mathbf{h}_j(t)$ for $j = 1, 2, \dots, N$.

The outward unit normal vector \mathbf{n}^h , the unit tangential vector $\boldsymbol{\tau}^h$, and the Cahn–Hoffman $\boldsymbol{\xi}$ -vector $\boldsymbol{\xi}^h$ of the curve $\Gamma^h(t)$ are constant vectors in the interior of each interval I_j which can be computed by $\mathbf{h}_j(t)$ as

$$(3.2) \quad \mathbf{n}^h|_{I_j} = -\frac{(\mathbf{h}_j)^\perp}{|\mathbf{h}_j|} := \mathbf{n}_j^h, \quad \boldsymbol{\tau}^h|_{I_j} = \frac{\mathbf{h}_j}{|\mathbf{h}_j|} := \boldsymbol{\tau}_j^h, \quad \boldsymbol{\xi}^h|_{I_j} = \boldsymbol{\xi}(\mathbf{n}_j^h) := \boldsymbol{\xi}_j^h.$$

Furthermore, for two scalar-/vector-valued functions u and v in \mathbb{K}^h or $[\mathbb{K}^h]^2$, respectively, the mass lumped inner product $(\cdot, \cdot)_{\Gamma^h}^h$ over Γ^h is defined as

$$(3.3) \quad (u, v)_{\Gamma^h}^h := \frac{1}{2} \sum_{j=1}^N |\mathbf{h}_j| \left[(u \cdot v)(\rho_j^-) + (u \cdot v)(\rho_{j-1}^+) \right],$$

where $u(\rho_j^\pm) = \lim_{\rho \rightarrow \rho_j^\pm} u(\rho)$ for $0 \leq j \leq N$.

Suppose $\Gamma^h(0) := \mathbf{X}^h(\mathbb{T}, 0)$, $\mathbf{X}^h(\cdot, 0) \in [\mathbb{K}^h]^2$ is the piecewise linear interpolation of $\mathbf{X}_0(s)$ in (1.7), where $\mathbf{X}^h(\rho = \rho_j, 0) = \mathbf{X}_0(s = s_j^0)$ with $s_j^0 = L_0 \rho_j$ for $j = 0, 1, \dots, N$. Now we can state the following spatial semidiscretization of the symmetrized variational formulation (2.11): for a given initial curve $\Gamma^h(0) := \mathbf{X}^h(\mathbb{T}, 0)$, $\mathbf{X}^h(\cdot, 0) \in [\mathbb{K}^h]^2$, find the solution $\Gamma^h(t) := \mathbf{X}^h(\mathbb{T}, t)$, $\mathbf{X}^h(\cdot, t) = (x^h(\cdot, t), y^h(\cdot, t))^T \in [\mathbb{K}^h]^2$ and $\mu^h(\cdot, t) \in \mathbb{K}^h$ such that

$$(3.4a) \quad \left(\mathbf{n}^h \cdot \partial_t \mathbf{X}^h, \varphi^h \right)_{\Gamma^h}^h + \left(\partial_s \mu^h, \partial_s \varphi^h \right)_{\Gamma^h}^h = 0 \quad \forall \varphi^h \in \mathbb{K}^h,$$

$$(3.4b) \quad \left(\mu^h, \mathbf{n}^h \cdot \boldsymbol{\omega}^h \right)_{\Gamma^h}^h - \left(\mathbf{Z}_k(\mathbf{n}^h) \partial_s \mathbf{X}^h, \partial_s \boldsymbol{\omega}^h \right)_{\Gamma^h}^h = 0 \quad \forall \boldsymbol{\omega}^h \in [\mathbb{K}^h]^2,$$

where

$$\begin{aligned} \mathbf{Z}_k(\mathbf{n}^h) &= \gamma(\mathbf{n}^h) I_2 - \mathbf{n}^h \boldsymbol{\xi}(\mathbf{n}^h)^T - \boldsymbol{\xi}(\mathbf{n}^h) (\mathbf{n}^h)^T + k(\mathbf{n}^h) \mathbf{n}^h (\mathbf{n}^h)^T \\ &= \gamma(\mathbf{n}^h) I_2 - \mathbf{n}^h (\boldsymbol{\xi}^h)^T - \boldsymbol{\xi}^h (\mathbf{n}^h)^T + k(\mathbf{n}^h) \mathbf{n}^h (\mathbf{n}^h)^T. \end{aligned}$$

Let $A^h(t)$ denote the area of the enclosed region of the piecewise linear closed curve $\Gamma^h(t)$ and let $W_c^h(t)$ be its total free energy; these are defined as

$$(3.5) \quad A^h(t) = \frac{1}{2} \sum_{j=1}^N [x_j^h(t) - x_{j-1}^h(t)] [y_j^h(t) + y_{j-1}^h(t)], \quad W_c^h(t) = \sum_{j=1}^N |\mathbf{h}_j(t)| \gamma(\mathbf{n}_j^h).$$

Remark 3.1. Similar to the proof in [29, Proposition 3.1], for the solution of the above semidiscretization (3.4), we can easily prove the area conservation and energy dissipation during time evolution.

3.2. A structure-preserving PFEM. Let $\tau > 0$ be the time step size and $t_m = m\tau$ be the discrete time levels for each $m \geq 0$. Let $\Gamma^m \triangleq \Gamma^{h,m} = \mathbf{X}^m(\mathbb{T})$, $\mathbf{X}^m(\cdot) = (x^m(\cdot), y^m(\cdot))^T \in [\mathbb{K}^h]^2$ be the numerical approximation of $\Gamma^h(t_m) = \mathbf{X}^h(\mathbb{T}, t_m)$, $\mathbf{X}^h(\cdot, t_m) \in [\mathbb{K}^h]^2$, and $\mu^m(\cdot) \in \mathbb{K}^h$ be the numerical approximation of $\mu^h(\cdot, t_m) \in \mathbb{K}^h$ for each $m \geq 0$, where $(\mathbf{X}^h(\cdot, t), \mu^h(\cdot, t))$ is the solution of the semidiscretization (3.4). Similarly, Γ^m is formed by the ordered vectors $\{\mathbf{h}_j^m\}_{j=1}^N$ defined by

$$(3.6) \quad \mathbf{h}_j^m := \mathbf{X}^m(\rho_j) - \mathbf{X}^m(\rho_{j-1}), \quad j = 1, 2, \dots, N.$$

Again, for each $m \geq 0$, the outward unit normal vector \mathbf{n}^m , the unit tangential vector $\boldsymbol{\tau}^m$, and the Cahn–Hoffman $\boldsymbol{\xi}$ -vector $\boldsymbol{\xi}^m$ of the curve Γ^m are constant vectors in the interior of each interval I_j which can be computed as

$$(3.7) \quad \mathbf{n}^m|_{I_j} = -\frac{(\mathbf{h}_j^m)^\perp}{|\mathbf{h}_j^m|} := \mathbf{n}_j^m, \quad \boldsymbol{\tau}^m|_{I_j} = \frac{\mathbf{h}_j^m}{|\mathbf{h}_j^m|} := \boldsymbol{\tau}_j^m, \quad \boldsymbol{\xi}^m|_{I_j} = \boldsymbol{\xi}(\mathbf{n}_j^m) := \boldsymbol{\xi}_j^m.$$

Following the idea in [5, 23] to design an SP-PFEM for surface diffusion, i.e., using the backward Euler method in time and the information of the curve at the current time step and the next time step to linearly interpolate the normal vector, a symmetrized SP-PFEM discretization of (3.4) is given as follows: for a given initial curve $\Gamma^0 := \mathbf{X}^0(\mathbb{T})$, $\mathbf{X}^0(\cdot) \in [\mathbb{K}^h]^2$, for $m \geq 0$, find the curve $\Gamma^{m+1} := \mathbf{X}^{m+1}(\mathbb{T})$, $\mathbf{X}^{m+1}(\cdot) \in [\mathbb{K}^h]^2$ and the chemical potential $\mu^{m+1}(\cdot) \in \mathbb{K}^h$, such that

$$(3.8a) \quad \left(\frac{\mathbf{X}^{m+1} - \mathbf{X}^m}{\tau} \cdot \mathbf{n}^{m+\frac{1}{2}}, \varphi^h \right)_{\Gamma^m}^h + \left(\partial_s \mu^{m+1}, \partial_s \varphi^h \right)_{\Gamma^m}^h = 0 \quad \forall \varphi^h \in \mathbb{K}^h,$$

$$(3.8b) \quad \left(\mu^{m+1}, \mathbf{n}^{m+\frac{1}{2}} \cdot \boldsymbol{\omega}^h \right)_{\Gamma^m}^h - \left(\mathbf{Z}_k(\mathbf{n}^m) \partial_s \mathbf{X}^{m+1}, \partial_s \boldsymbol{\omega}^h \right)_{\Gamma^m}^h = 0 \quad \forall \boldsymbol{\omega}^h \in [\mathbb{K}^h]^2,$$

where s is the arclength parameter of Γ^m , and $\mathbf{n}^{m+\frac{1}{2}}$ and $\mathbf{Z}_k(\mathbf{n}^m)$ are defined as

$$(3.9) \quad \mathbf{n}^{m+\frac{1}{2}} := -\frac{1}{2} (\partial_s \mathbf{X}^m + \partial_s \mathbf{X}^{m+1})^\perp = -\frac{1}{2} \frac{1}{|\partial_\rho \mathbf{X}^m|} (\partial_\rho \mathbf{X}^m + \partial_\rho \mathbf{X}^{m+1})^\perp,$$

$$(3.10) \quad \begin{aligned} \mathbf{Z}_k(\mathbf{n}^m) &= \gamma(\mathbf{n}^m) I_2 - \mathbf{n}^m \boldsymbol{\xi}(\mathbf{n}^m)^T - \boldsymbol{\xi}(\mathbf{n}^m) (\mathbf{n}^m)^T + k(\mathbf{n}^m) \mathbf{n}^m (\mathbf{n}^m)^T \\ &= \gamma(\mathbf{n}^m) I_2 - \mathbf{n}^m (\boldsymbol{\xi}^m)^T - \boldsymbol{\xi}^m (\mathbf{n}^m)^T + k(\mathbf{n}^m) \mathbf{n}^m (\mathbf{n}^m)^T, \end{aligned}$$

and for any scalar-/vector-valued function $f \in \mathbb{K}^h$ or $[\mathbb{K}^h]^2$, respectively, we compute its derivative with respect to the arclength parameter on Γ^m as $\partial_s f = |\partial_\rho \mathbf{X}^m|^{-1} \partial_\rho f$.

The above scheme is “weakly implicit” with only one nonlinear term introduced in (3.8a) and (3.8b), respectively. In particular, the nonlinear term is a polynomial function of degree at most two with respect to the components of \mathbf{X}^{m+1} and μ^{m+1} . Again, similar to [5] for surface diffusion, the fully implicit SP-PFEM (3.8) can be efficiently and accurately solved by the Newton’s iterative method in practical computations.

Remark 3.2. The choice of $\mathbf{n}^{m+\frac{1}{2}}$ in (3.8) plays an essential role in the proof of the area conservation, but it makes the numerical scheme fully implicit, i.e., a nonlinear system has to be solved at each time step. By replacing $\mathbf{n}^{m+1/2}$ with \mathbf{n}^m , we can easily construct a semi-implicit PFEM, where only a linear system has to be solved at each time step. Similar to the fully implicit SP-PFEM (3.8), the semi-implicit PFEM can also be proved to be unconditionally energy-stable if $\gamma(\mathbf{n})$ satisfies the condition (1.13). Of course, the semi-implicit PFEM does not conserve the area at the fully discrete level.

3.3. Main results. Let A^m be the area of the interior region of the piecewise linear closed curve Γ^m and let W_c^m ($m \geq 0$) be its energy; these are defined as

$$(3.11) \quad A^m := \frac{1}{2} \sum_{j=1}^N (x_j^m - x_{j-1}^m) (y_j^m + y_{j-1}^m), \quad W_c^m := W_c(\Gamma^m) = \sum_{j=1}^N |\mathbf{h}_j^m| \gamma(\mathbf{n}_j^m).$$

Denote

$$(3.12) \quad F(\mathbf{n}, \hat{\mathbf{n}}) = \frac{\gamma(\hat{\mathbf{n}})^2 - \gamma(\mathbf{n})^2 + 2\gamma(\mathbf{n})(\boldsymbol{\xi} \cdot \hat{\mathbf{n}}^\perp)(\mathbf{n} \cdot \hat{\mathbf{n}}^\perp)}{\gamma(\mathbf{n})(\mathbf{n} \cdot \hat{\mathbf{n}}^\perp)^2} \quad \forall \mathbf{n} \neq \pm \hat{\mathbf{n}} \in \mathbb{S}^1,$$

and define the minimal stabilizing function $k_0(\mathbf{n}) : \mathbb{S}^1 \rightarrow \mathbb{R}^+$ as (the existence will be given in the next section)

$$(3.13) \quad k_0(\mathbf{n}) := \max_{\hat{\mathbf{n}} \in \mathbb{S}^1} F(\mathbf{n}, \hat{\mathbf{n}}) \quad \text{with} \quad \mathbb{S}_\mathbf{n}^1 := \{\hat{\mathbf{n}} \in \mathbb{S}^1 \mid \hat{\mathbf{n}} \cdot \mathbf{n} \geq 0\}, \quad \mathbf{n} \in \mathbb{S}^1.$$

Then for the SP-PFEM (3.8), we have the following theorem.

THEOREM 3.1 (structure-preserving). *Assume $\gamma(\mathbf{n})$ satisfies (1.13) and take $k(\mathbf{n})$ in (2.1) satisfying $k(\mathbf{n}) \geq k_0(\mathbf{n})$ for $\mathbf{n} \in \mathbb{S}^1$; then the SP-PFEM (3.8) is area conservation and energy dissipation, i.e.,*

$$(3.14) \quad A^m \equiv A^0 = \frac{1}{2} \sum_{j=1}^N (x_j^0 - x_{j-1}^0) (y_j^0 + y_{j-1}^0), \quad m \geq 0.$$

$$(3.15) \quad W_c^{m+1} \leq W_c^m \leq \dots \leq W_c^0 = \sum_{j=1}^N |\mathbf{h}_j^0| \gamma(\mathbf{n}_j^0) \quad \forall m \geq 0.$$

The proof of area conservation (3.14) is similar to the proof in [5, Theorem 2.1] and it is omitted here for brevity, and we will establish the energy dissipation or unconditional energy stability (3.15) in the next section.

4. Energy dissipation. In this section, we first show, under the condition (1.13) on $\gamma(\mathbf{n})$, that the minimal stabilizing function $k_0(\mathbf{n})$ (3.13) is well defined, and then we prove the energy dissipation of the SP-PFEM (3.8).

4.1. Choice of the stabilizing function. The function $F(\mathbf{n}, \hat{\mathbf{n}})$ is continuous for $\mathbf{n} \neq \pm \hat{\mathbf{n}}$. Thus to show that the maximum in (3.13) is finite, it suffices to extend the definition of $F(\mathbf{n}, \hat{\mathbf{n}})$ to $\mathbf{n} = \pm \hat{\mathbf{n}}$.

THEOREM 4.1 (existence of limit). *For $\gamma(\mathbf{p}) \in C^2(\mathbb{R}^2 \setminus \{\mathbf{0}\})$, we have*

$$(4.1) \quad \lim_{\substack{\hat{\mathbf{n}} \rightarrow \mathbf{n} \\ \hat{\mathbf{n}} \in \mathbb{S}^1}} F(\mathbf{n}, \hat{\mathbf{n}}) = (\mathbf{n}^\perp)^T \mathbf{H}_\gamma(\mathbf{n}) \mathbf{n}^\perp + \frac{|\boldsymbol{\xi}|^2}{\gamma(\mathbf{n})} \quad \forall \mathbf{n} \in \mathbb{S}^1.$$

Proof. Plugging the vector decomposition $\gamma(\mathbf{n}) = \boldsymbol{\xi} \cdot \mathbf{n} = (\boldsymbol{\xi} \cdot \hat{\mathbf{n}}^\perp)(\mathbf{n} \cdot \hat{\mathbf{n}}^\perp) + (\boldsymbol{\xi} \cdot \hat{\mathbf{n}})(\mathbf{n} \cdot \hat{\mathbf{n}})$ and $1 = \mathbf{n} \cdot \mathbf{n} = (\mathbf{n} \cdot \hat{\mathbf{n}}^\perp)^2 + (\mathbf{n} \cdot \hat{\mathbf{n}})^2$ into (3.12), we get

$$(4.2) \quad \begin{aligned} F(\mathbf{n}, \hat{\mathbf{n}}) &= \frac{\gamma(\hat{\mathbf{n}})^2 - \gamma(\mathbf{n})^2 + 2\gamma(\mathbf{n})^2 - 2\gamma(\mathbf{n})(\boldsymbol{\xi} \cdot \hat{\mathbf{n}})(\mathbf{n} \cdot \hat{\mathbf{n}})}{\gamma(\mathbf{n})|\mathbf{n} - \hat{\mathbf{n}}|^2(1 - |\mathbf{n} - \hat{\mathbf{n}}|^2/4)} \\ &= \frac{\gamma(\hat{\mathbf{n}})^2 + \gamma(\mathbf{n})^2 - 2\gamma(\mathbf{n})(\boldsymbol{\xi} \cdot \hat{\mathbf{n}})(1 - |\mathbf{n} - \hat{\mathbf{n}}|^2/2)}{\gamma(\mathbf{n})|\mathbf{n} - \hat{\mathbf{n}}|^2(1 - |\mathbf{n} - \hat{\mathbf{n}}|^2/4)} \\ &= \frac{1}{1 - |\mathbf{n} - \hat{\mathbf{n}}|^2/4} \left[\frac{\gamma(\hat{\mathbf{n}})^2 - \gamma(\mathbf{n})^2 - 2\gamma(\mathbf{n})(\boldsymbol{\xi} \cdot (\hat{\mathbf{n}} - \mathbf{n}))}{\gamma(\mathbf{n})|\mathbf{n} - \hat{\mathbf{n}}|^2} + \boldsymbol{\xi} \cdot \hat{\mathbf{n}} \right]. \end{aligned}$$

Here we use the following equality:

$$\mathbf{n} \cdot \hat{\mathbf{n}} = \frac{|\mathbf{n}|^2 + |\hat{\mathbf{n}}|^2 - |\mathbf{n} - \hat{\mathbf{n}}|^2}{2} = 1 - \frac{|\mathbf{n} - \hat{\mathbf{n}}|^2}{2}.$$

Under the condition $\gamma(\mathbf{p}) \in C^2(\mathbb{R}^2 \setminus \{\mathbf{0}\})$, using Taylor expansion and noting $\nabla \gamma(\mathbf{p})^2 = 2\gamma(\mathbf{p})\nabla \gamma(\mathbf{p})$ and $\boldsymbol{\xi} = \nabla \gamma(\mathbf{p})|_{\mathbf{p}=\mathbf{n}}$, we obtain

$$\gamma(\mathbf{p})^2 - \gamma(\mathbf{n})^2 - 2\gamma(\mathbf{n})\boldsymbol{\xi} \cdot (\mathbf{p} - \mathbf{n}) = (\mathbf{p} - \mathbf{n})^T \left[\gamma(\mathbf{n})\mathbf{H}_\gamma(\mathbf{n}) + \boldsymbol{\xi}\boldsymbol{\xi}^T \right] (\mathbf{p} - \mathbf{n}) + o(|\mathbf{p} - \mathbf{n}|^2).$$

For any $\mathbf{n} \in \mathbb{S}^1$, noting that

$$\lim_{\substack{\mathbf{p} \rightarrow \mathbf{n}^+ \\ \mathbf{p} \in \mathbb{S}^1}} \frac{\mathbf{p} - \mathbf{n}}{|\mathbf{p} - \mathbf{n}|} = \mathbf{n}^\perp, \quad \lim_{\substack{\mathbf{p} \rightarrow \mathbf{n}^- \\ \mathbf{p} \in \mathbb{S}^1}} \frac{\mathbf{p} - \mathbf{n}}{|\mathbf{p} - \mathbf{n}|} = -\mathbf{n}^\perp,$$

where $\mathbf{p} \rightarrow \mathbf{n}^+/\mathbf{n}^-$ means $\mathbf{p} \cdot \mathbf{n}^\perp \geq 0/\leq 0$, respectively. We then get

$$\begin{aligned} \lim_{\substack{\mathbf{p} \rightarrow \mathbf{n}^+ \\ \mathbf{p} \in \mathbb{S}^1}} \frac{(\mathbf{p} - \mathbf{n})^T \left[\gamma(\mathbf{n})\mathbf{H}_\gamma(\mathbf{n}) + \boldsymbol{\xi}\boldsymbol{\xi}^T \right] (\mathbf{p} - \mathbf{n})}{|\mathbf{p} - \mathbf{n}|^2} &= (\mathbf{n}^\perp)^T \left[\gamma(\mathbf{n})\mathbf{H}_\gamma(\mathbf{n}) + \boldsymbol{\xi}\boldsymbol{\xi}^T \right] \mathbf{n}^\perp, \\ \lim_{\substack{\mathbf{p} \rightarrow \mathbf{n}^- \\ \mathbf{p} \in \mathbb{S}^1}} \frac{(\mathbf{p} - \mathbf{n})^T \left[\gamma(\mathbf{n})\mathbf{H}_\gamma(\mathbf{n}) + \boldsymbol{\xi}\boldsymbol{\xi}^T \right] (\mathbf{p} - \mathbf{n})}{|\mathbf{p} - \mathbf{n}|^2} &= -(\mathbf{n}^\perp)^T \left[\gamma(\mathbf{n})\mathbf{H}_\gamma(\mathbf{n}) + \boldsymbol{\xi}\boldsymbol{\xi}^T \right] (-\mathbf{n}^\perp) \\ &= (\mathbf{n}^\perp)^T \left[\gamma(\mathbf{n})\mathbf{H}_\gamma(\mathbf{n}) + \boldsymbol{\xi}\boldsymbol{\xi}^T \right] \mathbf{n}^\perp, \end{aligned}$$

and thus we have

$$(4.3) \quad \begin{aligned} \lim_{\substack{\mathbf{p} \rightarrow \mathbf{n} \\ \mathbf{p} \in \mathbb{S}^1}} \frac{\gamma(\mathbf{p})^2 - \gamma(\mathbf{n})^2 - 2\gamma(\mathbf{n})\boldsymbol{\xi} \cdot (\mathbf{p} - \mathbf{n})}{|\mathbf{p} - \mathbf{n}|^2} &= (\mathbf{n}^\perp)^T \left[\gamma(\mathbf{n})\mathbf{H}_\gamma(\mathbf{n}) + \boldsymbol{\xi}\boldsymbol{\xi}^T \right] \mathbf{n}^\perp \\ &= \gamma(\mathbf{n}) (\mathbf{n}^\perp)^T \mathbf{H}_\gamma(\mathbf{n}) \mathbf{n}^\perp + (\boldsymbol{\xi} \cdot \mathbf{n}^\perp)^2. \end{aligned}$$

Combining (4.2) and (4.3), noting (1.3) to get $\gamma(\mathbf{n}) = \boldsymbol{\xi} \cdot \mathbf{n}$, we obtain

$$\begin{aligned}
 \lim_{\substack{\hat{\mathbf{n}} \rightarrow \mathbf{n} \\ \hat{\mathbf{n}} \in \mathbb{S}^1}} F(\mathbf{n}, \hat{\mathbf{n}}) &= \frac{1}{\gamma(\mathbf{n})} \lim_{\substack{\mathbf{p} \rightarrow \mathbf{n} \\ \mathbf{p} \in \mathbb{S}^1}} \frac{\gamma(\mathbf{p})^2 - \gamma(\mathbf{n})^2 - 2\gamma(\mathbf{n})\boldsymbol{\xi} \cdot (\mathbf{p} - \mathbf{n})}{|\mathbf{p} - \mathbf{n}|^2} + \boldsymbol{\xi} \cdot \mathbf{n} \\
 &= (\mathbf{n}^\perp)^T \mathbf{H}_\gamma(\mathbf{n}) \mathbf{n}^\perp + \frac{(\boldsymbol{\xi} \cdot \mathbf{n}^\perp)^2}{\gamma(\mathbf{n})} + \boldsymbol{\xi} \cdot \mathbf{n} \\
 (4.4) \quad &= (\mathbf{n}^\perp)^T \mathbf{H}_\gamma(\mathbf{n}) \mathbf{n}^\perp + \frac{|\boldsymbol{\xi}|^2}{\gamma(\mathbf{n})}.
 \end{aligned}$$

The proof is completed. □

Under the condition (1.13), for any $\mathbf{n} \in \mathbb{S}^1$, it is easy to see that $F(\mathbf{n}, \hat{\mathbf{n}})$ is a continuous function for $\hat{\mathbf{n}} \in \mathbb{S}^1$ with $\hat{\mathbf{n}} \neq -\mathbf{n}$. Furthermore, if $\gamma(\mathbf{n}) = \gamma(-\mathbf{n})$, then we know $F(\mathbf{n}, \hat{\mathbf{n}}) \in C^1(\mathbb{S}^1 \times \mathbb{S}^1)$. This, together with the above theorem, suggests defining the following.

THEOREM 4.2 (existence of stabilizing function). *Under the condition (1.13) on $\gamma(\mathbf{n})$ and assuming $k(\mathbf{n}) \geq k_0(\mathbf{n})$ for $\mathbf{n} \in \mathbb{S}^1$ in (2.1), we have*

$$(4.5) \quad \gamma(\mathbf{n})[(\hat{\mathbf{n}}^\perp)^T \mathbf{Z}_k(\mathbf{n}) \hat{\mathbf{n}}^\perp] \geq \gamma(\hat{\mathbf{n}})^2 \quad \forall \mathbf{n}, \hat{\mathbf{n}} \in \mathbb{S}^1.$$

In addition, we have an alternative definition of $k_0(\mathbf{n})$ in (3.13) as

$$(4.6) \quad k_0(\mathbf{n}) = \inf \left\{ k(\mathbf{n}) \mid \gamma(\mathbf{n})[(\hat{\mathbf{n}}^\perp)^T \mathbf{Z}_k(\mathbf{n}) \hat{\mathbf{n}}^\perp] \geq \gamma(\hat{\mathbf{n}})^2 \quad \forall \hat{\mathbf{n}} \in \mathbb{S}^1 \right\}, \quad \mathbf{n} \in \mathbb{S}^1.$$

Proof. Assume $k(\mathbf{n}) \geq k_0(\mathbf{n})$ for $\mathbf{n} \in \mathbb{S}^1$. For any $\mathbf{n} \in \mathbb{S}^1$, when $\hat{\mathbf{n}} \in \mathbb{S}_\mathbf{n}^1$, i.e., $\hat{\mathbf{n}} \cdot \mathbf{n} \geq 0$, plugging (2.1) into the left-hand side of (4.5), noting (3.12) and (3.13), we have

$$\begin{aligned}
 \gamma(\mathbf{n})[(\hat{\mathbf{n}}^\perp)^T \mathbf{Z}_k(\mathbf{n}) \hat{\mathbf{n}}^\perp] &= \gamma(\mathbf{n})^2 - 2\gamma(\mathbf{n})(\boldsymbol{\xi} \cdot \hat{\mathbf{n}}^\perp)(\mathbf{n} \cdot \hat{\mathbf{n}}^\perp) + \gamma(\mathbf{n})k(\mathbf{n})(\mathbf{n} \cdot \hat{\mathbf{n}}^\perp)^2 \\
 &\geq \gamma(\mathbf{n})^2 - 2\gamma(\mathbf{n})(\boldsymbol{\xi} \cdot \hat{\mathbf{n}}^\perp)(\mathbf{n} \cdot \hat{\mathbf{n}}^\perp) + \gamma(\mathbf{n})k_0(\mathbf{n})(\mathbf{n} \cdot \hat{\mathbf{n}}^\perp)^2 \\
 &\geq \gamma(\mathbf{n})^2 - 2\gamma(\mathbf{n})(\boldsymbol{\xi} \cdot \hat{\mathbf{n}}^\perp)(\mathbf{n} \cdot \hat{\mathbf{n}}^\perp) + \gamma(\mathbf{n})F(\mathbf{n}, \hat{\mathbf{n}})(\mathbf{n} \cdot \hat{\mathbf{n}}^\perp)^2 \\
 (4.7) \quad &= \gamma(\hat{\mathbf{n}})^2.
 \end{aligned}$$

On the other hand, when $\hat{\mathbf{n}} \cdot \mathbf{n} < 0$, then $-\hat{\mathbf{n}} \cdot \mathbf{n} > 0$, from (4.7) by replacing $\hat{\mathbf{n}}$ by $-\hat{\mathbf{n}}$ and noting $\gamma(-\hat{\mathbf{n}}) = \gamma(\hat{\mathbf{n}})$, we have

$$(4.8) \quad \gamma(\mathbf{n})[(\hat{\mathbf{n}}^\perp)^T \mathbf{Z}_k(\mathbf{n}) \hat{\mathbf{n}}^\perp] = \gamma(\mathbf{n})[(-\hat{\mathbf{n}}^\perp)^T \mathbf{Z}_k(\mathbf{n}) (-\hat{\mathbf{n}}^\perp)] \geq \gamma(-\hat{\mathbf{n}})^2 = \gamma(\hat{\mathbf{n}})^2.$$

Combining (4.7) and (4.8), we get (4.5) immediately.

From the above proof, it is easy to see that

$$\gamma(\mathbf{n})[(\hat{\mathbf{n}}^\perp)^T \mathbf{Z}_{k_0}(\mathbf{n}) \hat{\mathbf{n}}^\perp] \geq \gamma(\hat{\mathbf{n}})^2 \quad \forall \mathbf{n}, \hat{\mathbf{n}} \in \mathbb{S}^1,$$

which implies

$$(4.9) \quad k_0(\mathbf{n}) \geq \inf \left\{ k(\mathbf{n}) \mid \gamma(\mathbf{n})[(\hat{\mathbf{n}}^\perp)^T \mathbf{Z}_k(\mathbf{n}) \hat{\mathbf{n}}^\perp] \geq \gamma(\hat{\mathbf{n}})^2 \quad \forall \hat{\mathbf{n}} \in \mathbb{S}^1 \right\} \quad \forall \mathbf{n} \in \mathbb{S}^1.$$

On the other hand, suppose $\mathbf{Z}_k(\mathbf{n})$ satisfies (4.5); then we have

$$(4.10) \quad \gamma(\mathbf{n}) \left(\gamma(\mathbf{n}) - 2(\boldsymbol{\xi} \cdot \hat{\mathbf{n}}^\perp)(\mathbf{n} \cdot \hat{\mathbf{n}}^\perp) + k(\mathbf{n})(\mathbf{n} \cdot \hat{\mathbf{n}}^\perp)^2 \right) \geq \gamma(\hat{\mathbf{n}})^2 \quad \forall \hat{\mathbf{n}} \in \mathbb{S}_\mathbf{n}^1,$$

which implies

$$(4.11) \quad k(\mathbf{n}) \geq \frac{\gamma(\hat{\mathbf{n}})^2 - \gamma(\mathbf{n})^2 + 2\gamma(\mathbf{n})(\boldsymbol{\xi} \cdot \hat{\mathbf{n}}^\perp)(\mathbf{n} \cdot \hat{\mathbf{n}}^\perp)}{\gamma(\mathbf{n})(\mathbf{n} \cdot \hat{\mathbf{n}}^\perp)^2} = F(\mathbf{n}, \hat{\mathbf{n}}) \quad \forall \hat{\mathbf{n}} \in \mathbb{S}_\mathbf{n}^1.$$

By condition (1.13), this inequality holds for all $\hat{\mathbf{n}} \in \mathbb{S}^1$. Thus we get $k(\mathbf{n}) \geq k_0(\mathbf{n})$, which implies

$$(4.12) \quad k_0(\mathbf{n}) \leq \inf \left\{ k(\mathbf{n}) \mid \gamma(\mathbf{n})[(\hat{\mathbf{n}}^\perp)^T \mathbf{Z}_k(\mathbf{n}) \hat{\mathbf{n}}^\perp] \geq \gamma(\hat{\mathbf{n}})^2 \quad \forall \hat{\mathbf{n}} \in \mathbb{S}^1 \right\} \quad \forall \mathbf{n} \in \mathbb{S}^1.$$

Combining (4.9) and (4.12), we obtain (4.6) immediately. \square

Remark 4.1. Assume $\mathbf{n} = (-\sin \theta, \cos \theta)^T$ ($\theta \in [-\pi, \pi]$) and $\hat{\mathbf{n}} = (-\sin \hat{\theta}, \cos \hat{\theta})^T$; then the problem to find the minimal stabilizing function $k_0(\mathbf{n})$ defined in (3.13) can be reformulated as an optimization problem in terms of the single variable $\hat{\theta}$, i.e.,

$$(4.13) \quad \tilde{k}_0(\theta) := k_0(\mathbf{n}) = k_0(-\sin \theta, \cos \theta) = \max_{\hat{\theta} \in [\theta - \frac{\pi}{2}, \theta + \frac{\pi}{2}]} \tilde{F}^\theta(\hat{\theta}), \quad -\pi \leq \theta \leq \pi,$$

where

$$(4.14) \quad \tilde{F}^\theta(\hat{\theta}) := F(\mathbf{n}, \hat{\mathbf{n}}) = \frac{\hat{\gamma}(\hat{\theta})^2 - \hat{\gamma}(\theta)^2 - 2\hat{\gamma}(\theta)\hat{\gamma}'(\theta) \cos(\hat{\theta} - \theta) \sin(\hat{\theta} - \theta)}{\hat{\gamma}(\theta) \sin^2(\hat{\theta} - \theta)} + 2\hat{\gamma}(\theta),$$

with $\hat{\gamma}(\theta) := \gamma(\mathbf{n}) = \gamma(-\sin \theta, \cos \theta)$ and $\hat{\gamma}(\hat{\theta}) := \gamma(\hat{\mathbf{n}}) = \gamma(-\sin \hat{\theta}, \cos \hat{\theta})$ by noting $\boldsymbol{\xi} = \boldsymbol{\xi}(\mathbf{n}) = \hat{\gamma}(\theta)\mathbf{n} - \hat{\gamma}'(\theta)\mathbf{n}^\perp$. Thus for a given \mathbf{n} (or θ), we can obtain $k_0(\mathbf{n})$ (or $k_0(\theta)$) by numerically solving the above single-variable optimization problem (4.13).

COROLLARY 4.3 (positivity of the minimal stabilizing function). *Assume (4.5) is satisfied; then $\mathbf{Z}_k(\mathbf{n})$ is a symmetric positive definite matrix and*

$$(4.15) \quad \gamma(-\mathbf{n}) = \gamma(\mathbf{n}), \quad k_0(\mathbf{n}) > 0, \quad \forall \mathbf{n} \in \mathbb{S}^1.$$

Proof. Taking $\hat{\mathbf{n}} = -\mathbf{n}$ in (4.5), noting the first equality in (4.7), we get $\gamma(\mathbf{n})^2 \geq \gamma(-\mathbf{n})^2$, which suggests $\gamma(-\mathbf{n})^2 \geq \gamma(-(-\mathbf{n}))^2 = \gamma(\mathbf{n})^2$, and thus we obtain the first equality in (4.15) since $\gamma(\mathbf{n}) > 0$. From (4.5), we get $\mathbf{Z}_k(\mathbf{n})$ is symmetric positive definite, which implies $k(\mathbf{n}) = \text{Tr}(\mathbf{Z}_k(\mathbf{n})) \geq k_0(\mathbf{n}) = \text{Tr}(\mathbf{Z}_{k_0}(\mathbf{n})) > 0$ for $\mathbf{n} \in \mathbb{S}^1$. \square

If we consider from the anisotropic surface energy $\gamma(\mathbf{n})$ to its corresponding minimal stabilizing function $k_0(\mathbf{n})$ defined in (4.6) (or (3.13)) as a mapping, then it is a sublinear mapping, i.e., positively homogeneous and subadditive.

LEMMA 4.4 (positive homogeneity and subadditivity). *Assume $k_0(\mathbf{n})$, $k_1(\mathbf{n})$, and $k_2(\mathbf{n})$ be the minimal stabilizing functions for the anisotropic surface energies $\gamma(\mathbf{n})$, $\gamma_1(\mathbf{n})$, and $\gamma_2(\mathbf{n})$, respectively; then we have*

- (i) if $\gamma_1(\mathbf{n}) = c\gamma(\mathbf{n})$ with $c > 0$, then $k_1(\mathbf{n}) = ck_0(\mathbf{n})$ for $\mathbf{n} \in \mathbb{S}^1$, and
- (ii) if $\gamma(\mathbf{n}) = \gamma_1(\mathbf{n}) + \gamma_2(\mathbf{n})$, then $k_0(\mathbf{n}) \leq k_1(\mathbf{n}) + k_2(\mathbf{n})$ for $\mathbf{n} \in \mathbb{S}^1$.

Proof. From (1.3), we get

$$(4.16) \quad \boldsymbol{\xi} = \nabla\gamma(\mathbf{p})|_{\mathbf{p}=\mathbf{n}}, \quad \boldsymbol{\xi}_1 = \nabla\gamma_1(\mathbf{p})|_{\mathbf{p}=\mathbf{n}}, \quad \boldsymbol{\xi}_2 = \nabla\gamma_2(\mathbf{p})|_{\mathbf{p}=\mathbf{n}}.$$

(i) If $\gamma_1(\mathbf{n}) = c\gamma(\mathbf{n})$, we get $\boldsymbol{\xi}_1 = c\boldsymbol{\xi}$. This, together with (3.12), implies

$$(4.17) \quad F_1(\mathbf{n}, \hat{\mathbf{n}}) = \frac{\gamma_1(\hat{\mathbf{n}})^2 - \gamma_1(\mathbf{n})^2 + 2\gamma_1(\mathbf{n})(\boldsymbol{\xi}_1 \cdot \hat{\mathbf{n}}^\perp)(\mathbf{n} \cdot \hat{\mathbf{n}}^\perp)}{\gamma_1(\mathbf{n})(\mathbf{n} \cdot \hat{\mathbf{n}}^\perp)^2} = cF(\mathbf{n}, \hat{\mathbf{n}}).$$

Combining (4.17) and (3.13), we obtain the positive homogeneity immediately.

(ii) If $\gamma(\mathbf{n}) = \gamma_1(\mathbf{n}) + \gamma_2(\mathbf{n})$, then $\boldsymbol{\xi} = \boldsymbol{\xi}_1 + \boldsymbol{\xi}_2$; thus we have

$$\begin{aligned} \mathbf{Z}_{k_1+k_2}(\mathbf{n}) &= \gamma(\mathbf{n})I_2 - \boldsymbol{\xi}\mathbf{n}^T - \mathbf{n}\boldsymbol{\xi}^T + (k_1(\mathbf{n}) + k_2(\mathbf{n}))\mathbf{n}\mathbf{n}^T \\ &= \mathbf{Z}_{k_1}^{(1)}(\mathbf{n}) + \mathbf{Z}_{k_2}^{(2)}(\mathbf{n}), \end{aligned}$$

where

$$\begin{aligned} \mathbf{Z}_{k_1}^{(1)}(\mathbf{n}) &= \gamma_1(\mathbf{n})I_2 - \boldsymbol{\xi}_1\mathbf{n}^T - \mathbf{n}(\boldsymbol{\xi}_1)^T + k_1(\mathbf{n})\mathbf{n}\mathbf{n}^T, \\ \mathbf{Z}_{k_2}^{(2)}(\mathbf{n}) &= \gamma_2(\mathbf{n})I_2 - \boldsymbol{\xi}_2\mathbf{n}^T - \mathbf{n}(\boldsymbol{\xi}_2)^T + k_2(\mathbf{n})\mathbf{n}\mathbf{n}^T. \end{aligned}$$

By using the Cauchy inequality, we get

$$\begin{aligned} &\gamma(\mathbf{n})[(\hat{\mathbf{n}}^\perp)^T \mathbf{Z}_{k_1+k_2}(\mathbf{n}) \hat{\mathbf{n}}^\perp] \\ &\geq \left(\sqrt{\gamma_1(\mathbf{n})[(\hat{\mathbf{n}}^\perp)^T \mathbf{Z}_{k_1}^{(1)}(\mathbf{n}) \hat{\mathbf{n}}^\perp]} + \sqrt{\gamma_2(\mathbf{n})[(\hat{\mathbf{n}}^\perp)^T \mathbf{Z}_{k_2}^{(2)}(\mathbf{n}) \hat{\mathbf{n}}^\perp]} \right)^2 \\ (4.18) \quad &\geq (\gamma_1(\hat{\mathbf{n}}) + \gamma_2(\hat{\mathbf{n}}))^2 = \gamma(\hat{\mathbf{n}})^2. \end{aligned}$$

Combining (4.18) and (4.6), we get $k_0(\mathbf{n}) \leq k_1(\mathbf{n}) + k_2(\mathbf{n})$ for $\mathbf{n} \in \mathbb{S}^1$. □

4.2. Energy dissipation. For the SP-PFEM (3.8), we have the following.

THEOREM 4.5 (energy dissipation). *Assume the surface energy matrix $\mathbf{Z}_k(\mathbf{n})$ satisfies (4.5); then the SP-PFEM (3.8) is unconditionally energy-stable, i.e., for any $\tau > 0$, we have*

$$(4.19) \quad W_c^{m+1} \leq W_c^m \leq \dots \leq W_c^0 = \sum_{j=1}^N |\mathbf{h}_j^0| \gamma(\mathbf{n}_j^0) \quad \forall m \geq 0.$$

Proof. Under (4.5), we know that $\mathbf{Z}_k(\mathbf{n})$ is symmetric positive definite. Thus we have

$$(4.20) \quad \left(\mathbf{Z}_k(\mathbf{n})\mathbf{u}, \mathbf{u} - \mathbf{v} \right) \geq \frac{1}{2} \left(\mathbf{Z}_k(\mathbf{n})\mathbf{u}, \mathbf{u} \right) - \frac{1}{2} \left(\mathbf{Z}_k(\mathbf{n})\mathbf{v}, \mathbf{v} \right) \quad \forall \mathbf{u}, \mathbf{v} \in \mathbb{R}^2.$$

Using (2.4) and $\boldsymbol{\xi} \cdot \mathbf{n} = \gamma(\mathbf{n})$, we get

$$(4.21) \quad (\partial_s \mathbf{X}^m)^T \mathbf{Z}_k(\mathbf{n}^m) \partial_s \mathbf{X}^m = \boldsymbol{\tau}^m \cdot (\boldsymbol{\xi}^m)^\perp = \gamma(\mathbf{n}^m).$$

Combining (4.21) and (4.20), noting $\mathbf{Z}_k(\mathbf{n})$ satisfies (4.5), we obtain

$$\begin{aligned} &\left(\mathbf{Z}_k(\mathbf{n}^m) \partial_s \mathbf{X}^{m+1}, \partial_s \mathbf{X}^{m+1} - \partial_s \mathbf{X}^m \right)_{\Gamma^m}^h + \int_{\Gamma^m} \gamma(\mathbf{n}^m) ds \\ &\geq \frac{1}{2} \left(\mathbf{Z}_k(\mathbf{n}^m) \partial_s \mathbf{X}^{m+1}, \partial_s \mathbf{X}^{m+1} \right)_{\Gamma^m}^h + \frac{1}{2} \int_{\Gamma^m} \gamma(\mathbf{n}^m) ds \\ &= \sum_{j=1}^N \frac{(\mathbf{h}_j^{m+1})^T \mathbf{Z}_k(\mathbf{n}_j^m) \mathbf{h}_j^{m+1} + \gamma(\mathbf{n}_j^m) |\mathbf{h}_j^m|^2}{2|\mathbf{h}_j^m|} \\ &\geq \sum_{j=1}^N |\mathbf{h}_j^{m+1}| \sqrt{\left((\mathbf{n}_j^{m+1})^\perp \right)^T \mathbf{Z}_k(\mathbf{n}_j^m) (\mathbf{n}_j^{m+1})^\perp \gamma(\mathbf{n}_j^m)} \\ (4.22) \quad &\geq \sum_{j=1}^N |\mathbf{h}_j^{m+1}| \sqrt{\frac{\gamma^2(\mathbf{n}_j^{m+1})}{\gamma(\mathbf{n}_j^m)} \gamma(\mathbf{n}_j^m)} = \sum_{j=1}^N |\mathbf{h}_j^{m+1}| \gamma(\mathbf{n}_j^{m+1}) = \int_{\Gamma^{m+1}} \gamma(\mathbf{n}^{m+1}) ds. \end{aligned}$$

Taking $\varphi^h = \mu^{m+1}$ in (3.8a) and $\omega^h = \mathbf{X}^{m+1} - \mathbf{X}^m$ in (3.8b) and combining with the inequality (4.22), we get

$$\begin{aligned} W_c^{m+1} - W_c^m &= \int_{\Gamma^{m+1}} \gamma(\mathbf{n}^{m+1}) ds - \int_{\Gamma^m} \gamma(\mathbf{n}^m) ds \\ &\leq \left(\mathbf{Z}_k(\mathbf{n}^m) \partial_s \mathbf{X}^{m+1}, \partial_s \mathbf{X}^{m+1} - \partial_s \mathbf{X}^m \right)_{\Gamma^m}^h \\ (4.23) \quad &= -\tau \left(\partial_s \mu^{m+1}, \partial_s \mu^{m+1} \right)_{\Gamma^m}^h \leq 0 \quad \forall m \geq 0, \end{aligned}$$

which implies the energy dissipation (4.19) for the SP-PFEM (3.8). \square

Combining Theorems 4.2 and 4.6, finally we have the following corollary.

COROLLARY 4.6 (energy dissipation). *Assume $\gamma(\mathbf{n})$ satisfies (1.13), and taking $k(\mathbf{n}) \geq k_0(\mathbf{n})$ in (2.1), then the SP-PFEM (3.8) is unconditionally energy-stable.*

4.3. Explicit formulas for the minimal stabilizing function. Here we give explicit formulas of the minimal stabilizing function $k_0(\mathbf{n})$ for several popular anisotropic surface energies $\gamma(\mathbf{n})$ in applications. Denote

$$\mathbf{J} = \begin{pmatrix} 0 & -1 \\ 1 & 0 \end{pmatrix}, \quad \mathbf{Z}_0(\mathbf{n}) = \begin{pmatrix} 1 & n_1 n_2 \\ n_1 n_2 & 1 \end{pmatrix}, \quad \forall \mathbf{n} = \begin{pmatrix} n_1 \\ n_2 \end{pmatrix} \in \mathbb{S}^1.$$

LEMMA 4.7 (Riemannian-like metric). *When $\gamma(\mathbf{n})$ is taken as the Riemannian-like metric anisotropic surface energy (1.8), we have $k_0(\mathbf{n}) \leq k_1(\mathbf{n})$, where*

$$(4.24) \quad k_1(\mathbf{n}) = \sum_{l=1}^L \gamma_l(\mathbf{n})^{-1} \text{Tr}(\mathbf{G}_l), \quad \mathbf{Z}_{k_1}(\mathbf{n}) = \sum_{l=1}^L \gamma_l(\mathbf{n})^{-1} \mathbf{J}^T \mathbf{G}_l \mathbf{J}, \quad \forall \mathbf{n} \in \mathbb{S}^1,$$

and $k_0(\mathbf{n}) = k_1(\mathbf{n})$ if $L = 1$.

The proof can be found in Appendix B.

Remark 4.2. By taking $k(\mathbf{n}) = k_1(\mathbf{n})$ in (2.1) and using the semi-implicit discretization \mathbf{n}^m instead of $\mathbf{n}^{m+\frac{1}{2}}$, the SP-PFEM (3.8) collapses to the BGN formulation used in [7].

LEMMA 4.8 (l^r -norm metric). *When $\gamma(\mathbf{n})$ is taken as the l^r -norm metric anisotropic surface energy (1.9), we have*

- (i) when $r = 4$, $k_0(\mathbf{n}) = 2\gamma(\mathbf{n})^{-3}$ and $\mathbf{Z}_{k_0}(\mathbf{n}) = \gamma(\mathbf{n})^{-3} \mathbf{Z}_0(\mathbf{n})$, and
- (ii) when $r = 6$, $k_0(\mathbf{n}) = 2\gamma(\mathbf{n})^{-5} (n_1^4 + n_1^2 n_2^2 + n_2^4)$.

The proof can be found in Appendix C.

LEMMA 4.9 (m -fold). *When $\gamma(\mathbf{n})$ is taken as the m -fold anisotropy (1.10), we have*

- (i) when $\gamma(\mathbf{n}) = 1 + \beta \cos 2\theta$, then

$$(4.25) \quad k_0(\mathbf{n}) = 4 - 2\gamma(\mathbf{n}) + \frac{4\beta^2}{\gamma(\mathbf{n})}; \text{ and}$$

- (ii) when $\gamma(\mathbf{n}) = 1 + \beta \cos 4\theta$, then

$$(4.26) \quad k_0(\mathbf{n}) \leq 2\gamma(\mathbf{n}) + \frac{16\beta + 16\beta^2}{\gamma(\mathbf{n})} := k_1(\mathbf{n}).$$

The proof can be found in Appendix D.

5. Numerical results. In this section, we numerically implement the SP-PFEM (3.8) for simulating the evolution of closed curves under anisotropic surface diffusion. Numerical results demonstrate the high performance of the proposed scheme, e.g., the spatial/temporal convergence rates, energy dissipation, area conservation, and asymptotic quasi-uniform mesh distribution. Here, the distance between two closed curves Γ_1 and Γ_2 is measured by the manifold distance $M(\Gamma_1, \Gamma_2)$ which was introduced in the reference [47].

Since formally the scheme is first-order accurate in time and second-order accurate in space, the mesh size h and the time step τ are chosen as $\tau = \mathcal{O}(h^2)$, e.g., $\tau = h^2$, except where noted. Let Γ^m be the numerical approximation of $\Gamma^h(t = t_m = m\tau)$ with mesh size h and time step τ ; the numerical error is then measured as

$$(5.1) \quad e^h(t_m) := M(\Gamma^m, \Gamma(t = t_m)), \quad m \geq 0.$$

Because the exact solution cannot be obtained analytically, we choose fine meshes $h = h_e$, $\tau = \tau_e$ to obtain $\Gamma(t = t_m)$ numerically, e.g., $h_e = 2^{-8}$ and $\tau_e = 2^{-16}$.

The normalized area loss and the mesh ratio $R^h(t_m)$, which indicates the mesh quality during evolution, are defined as

$$(5.2) \quad \frac{\Delta A^h(t_m)}{A^h(0)} := \frac{A^h(t_m) - A^h(0)}{A^h(0)}, \quad R^h(t_m) := \frac{\max_{1 \leq j \leq N} |\mathbf{h}_j^m|}{\min_{1 \leq j \leq N} |\mathbf{h}_j^m|}, \quad m \geq 0,$$

where $A^h(t_m)$ is the area of the inner region enclosed by Γ^m .

In the following simulations, the initial shape in (1.7) is always chosen as an ellipse with length 4 and width 1 except where noted, and the tolerance of the Newton iteration in the SP-PFEM (3.8) is chosen as 10^{-12} .

5.1. Convergence rates and energy dissipation. In order to test convergence rates of the SP-PFEM (3.8), without loss of generality, we choose the following two kinds of anisotropic surface energies:

- Case I: The Riemannian-like metric anisotropic surface energy (1.8) with $L = 1$ and $\mathbf{G}_1 = \text{diag}(1, 2) := \mathbf{G}$ and the corresponding minimal stabilizing function $k_0(\mathbf{n})$ are given explicitly in (4.24).
- Case II: The l^r -norm metric anisotropic surface energy (1.9) with $r = 4$ and the corresponding minimal stabilizing function $k_0(\mathbf{n})$ are given explicitly in Lemma 4.8.

Figure 5.1 plots spatial convergence rates of the SP-PFEM at different times under a fixed value $k(\mathbf{n})$ in (2.1) or different values of $k(\mathbf{n})$ under a fixed time $t = 0.5$. Figure 5.2 depicts time evolution of the normalized area loss and the normalized energy under different parameters. Figure 5.3 depicts time evolution of the mesh ratio $R^h(t)$ under different mesh sizes h , time steps τ , and $k(\mathbf{n})$ for the above two cases.

From Figures 5.1–5.3, we can obtain the following results for the SP-PFEM (3.8) for simulating anisotropic surface diffusion of closed curves:

- (i) The SP-PFEM is second-order accurate in space (cf. Figure 5.1).
- (ii) The area is conserved numerically up to the round-off error around 10^{-16} (cf. Figure 5.2(a) and (d)).
- (iii) The number of Newton iterations at each time step is around 2 to 4; thus it is very efficient (cf. Figure 5.2(a) and (d)).
- (iv) The SP-PFEM is unconditionally energy-stable when $k(\mathbf{n})$ satisfies the energy dissipation condition in Theorem 4.5 (cf. Figure 5.2(b)–(c) and (e)–(f)).

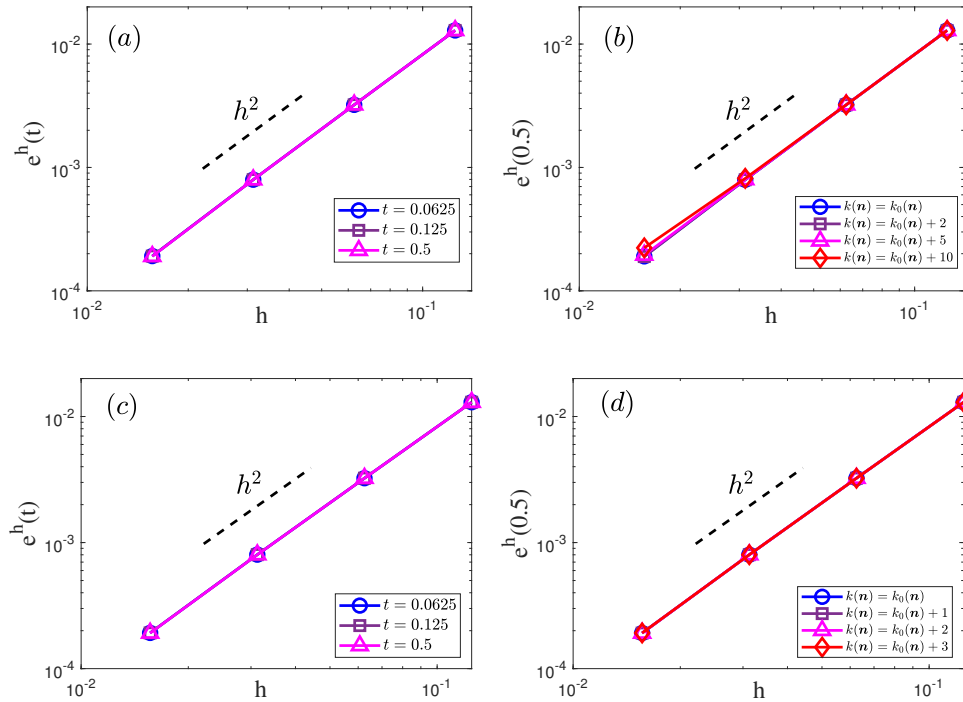


FIG. 5.1. Spatial convergence rates of the SP-PFEM (3.8) for Case I at different times with $k(\mathbf{n}) = k_0(\mathbf{n})$ in (4.24) (a), and at time $t = 0.5$ for different $k(\mathbf{n})$ (b), and for Case II at different times with $k(\mathbf{n}) = k_0(\mathbf{n})$ in Lemma 4.8 (c), and at time $t = 0.5$ for different $k(\mathbf{n})$ (d).

(v) The mesh ratio $R^h(t = t_m)$ approaches a constant C when $t \gg 1$ for each case, which indicates asymptotic quasi-uniform mesh distribution, no matter what kind of anisotropic surface energy is used as long as it is weakly anisotropic.

5.2. Application for morphological evolutions. Here, we use the SP-PFEM (3.8) to simulate the morphological evolution under different anisotropic surface energies, i.e., morphological evolutions of closed curves from a 4×1 rectangle toward their corresponding equilibrium shapes. Figure 5.4 depicts morphological evolutions for the four different weakly anisotropic surface energies including (a) the regularized l^1 -norm metric (1.11) with $\varepsilon = 0.1$ by taking $k(\mathbf{n}) = k_1(\mathbf{n}) := \frac{1.01}{\sqrt{n_1^2 + 0.01n_2^2}} + \frac{1.01}{\sqrt{0.01n_1^2 + n_2^2}}$, (b) the l^4 -norm metric (1.9) with $r = 4$ and $k(\mathbf{n}) = k_0(\mathbf{n})$ given in Lemma 4.10, (c) 2-fold anisotropic energy (1.10) with $m = 2$, $\theta_0 = \frac{\pi}{2}$, and $\beta = \frac{1}{3}$ and $k(\mathbf{n}) = k_0(\mathbf{n})$ given in (4.25), and (d) the Riemannian-like metric (1.8) with $L = 1$ and $\mathbf{G}_1 = \text{diag}(1, 2) := \mathbf{G}$ and $k(\mathbf{n}) = k_0(\mathbf{n})$ given in (4.24). Figures 5.5 and 5.6 show morphological evolutions and the normalized energy $\frac{W_c^h(t)}{W_c^h(0)}$ under the 2-fold $\gamma(\mathbf{n}) = 1 + \frac{3}{5} \cos(2\theta)$ and the 4-fold $\gamma(\mathbf{n}) = 1 + \frac{3}{10} \cos(4\theta)$, with $k(\mathbf{n})$ given in (4.25), (4.26), respectively, which are both strongly anisotropic surface energies. The Frank diagrams of the above anisotropic energies are all shown in Figure 5.7.

As shown in Figure 5.4(a)–(b), if we choose the anisotropy as the regularized l^1 -norm metric or the l^4 -norm metric, the equilibrium shapes are almost “faceting” squares; for 2-fold anisotropy (cf. Figure 5.4(c)), the number of edges in its equilibrium shape is exactly two; and for the Riemannian-like metric anisotropic energy (cf.

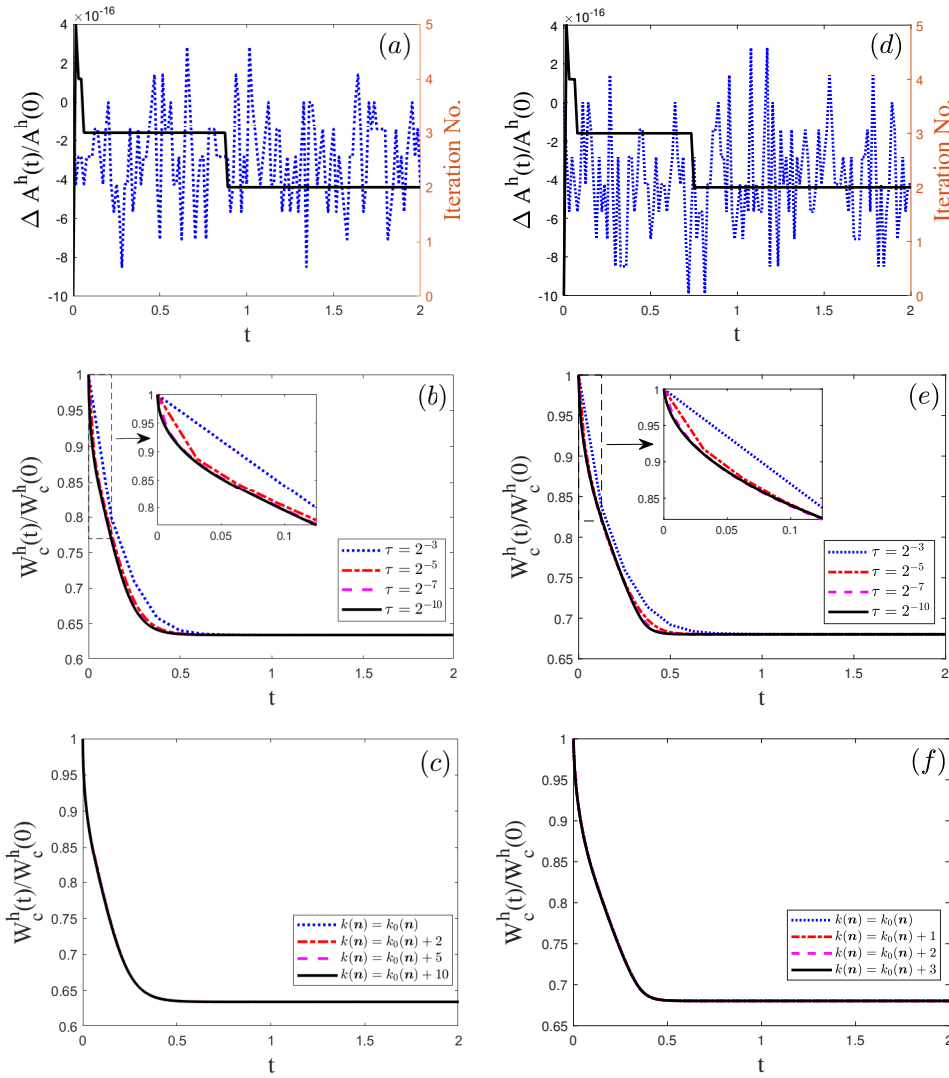


FIG. 5.2. Time evolution of the normalized area loss $\frac{\Delta A^h(t)}{A^h(0)}$ (first row, blue dashed line) and iteration number (first row, black line) and the normalized energy $\frac{W_c^h(t)}{W_c^h(0)}$ (second and third rows) for Case I with $k(\mathbf{n}) = k_0(\mathbf{n})$ in (4.24) for $h = 2^{-3}$ (a), with $h = 2^{-3}$ for different τ (b), and with $h = 2^{-3}$ for different $k(\mathbf{n})$ (c), and for Case II with $k(\mathbf{n}) = k_0(\mathbf{n})$ in Lemma 4.8 for $h = 2^{-3}$ (d), with $h = 2^{-3}$ for different τ (e), and with $h = 2^{-3}$ for different $k(\mathbf{n})$ (f).

Figure 5.4(d), the equilibrium shape is an ellipse. The numerical results are perfectly consistent with the theoretical predictions by the well-known Wulff construction [42, 7, 3]. Because the anisotropic surface diffusion is area preserving during the evolution, we can easily obtain its theoretical equilibrium shape (or Wulff shape) by using the expression in [3, 24]. As shown in Figures 5.5(h) and 5.6(h), the numerical equilibrium shapes are again perfectly consistent with the theoretical predictions by the Wulff construction in the strongly anisotropic cases. Meanwhile, we can clearly see

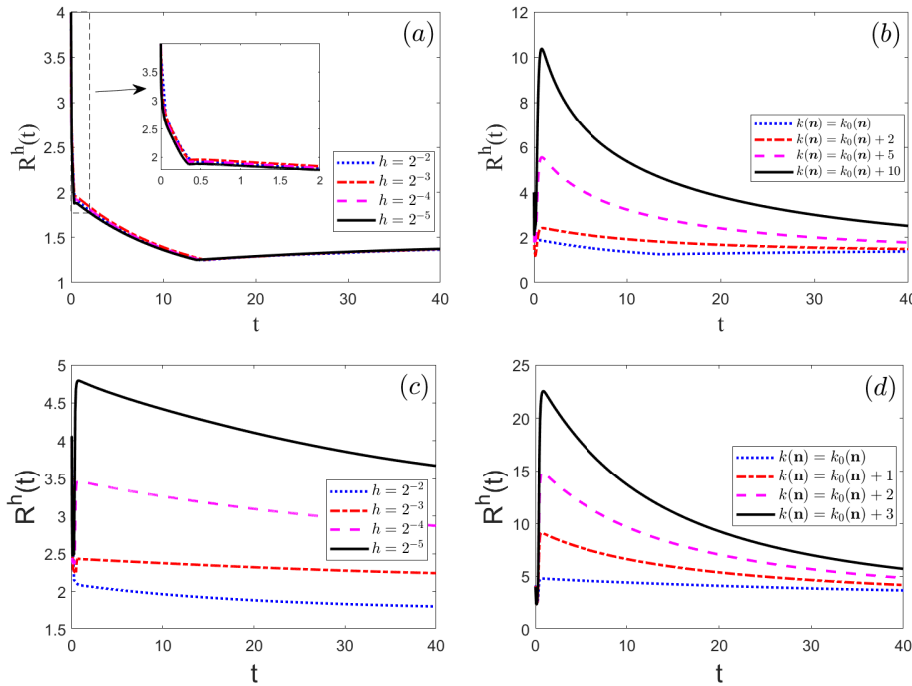


FIG. 5.3. Time evolution of the mesh ratio $R^h(t)$ for Case I with $k(\mathbf{n}) = k_0(\mathbf{n})$ in (4.24) for different h (a) and with $h = 2^{-5}$ for different $k(\mathbf{n})$ (b), and for Case II with $k(\mathbf{n}) = k_0(\mathbf{n})$ in Lemma 4.8 for different h (c) and with $h = 2^{-5}$ for different $k(\mathbf{n})$ (d).

that the normalized energy is monotonically decreasing during the evolution for the strongly anisotropic cases. Furthermore, we observe that the numerical equilibrium has several “cusps,” which result from the self-intersection of the Wulff envelope [3].

6. Conclusions. By utilizing a symmetric positive definite surface energy matrix $\mathbf{Z}_k(\mathbf{n})$ and a stabilizing function $k(\mathbf{n})$, we reformulated the anisotropic surface diffusion equation with any arbitrary anisotropic surface energy $\gamma(\mathbf{n})$ into a novel symmetrized form and derived a new variational formulation. We discretized the variational problem in space by the PFEM. For temporal discretization, we proposed a fully implicit SP-PFEM, which can rigorously preserve the total area up to machine precision. Then we rigorously proved that the proposed SP-PFEM is unconditionally energy-stable under a simple and mild condition (1.13) on the anisotropic surface energy $\gamma(\mathbf{n})$. Finally, numerical results demonstrated that the SP-PFEM is second-order accurate in space, is first-order in time, is unconditionally energy-stable, and enjoys very good mesh quality during the evolution, and no mesh redistribution procedure is needed even for strongly anisotropic cases. Another important contribution is that the new scheme can also work well for the strongly anisotropic cases (shown in Figures 5.5–5.6). In the existing literature, a Willmore regularization energy term is often added into the model to deal with the strongly anisotropic cases [33, 28, 18, 38, 24], but here we use only one unified scheme to tackle the two cases. In the future, we will further explore the high performance of the schemes, especially for the strongly anisotropic cases, and extend the new variational formulation to anisotropic surface diffusion of open/closed surfaces in three dimensions [26, 46].

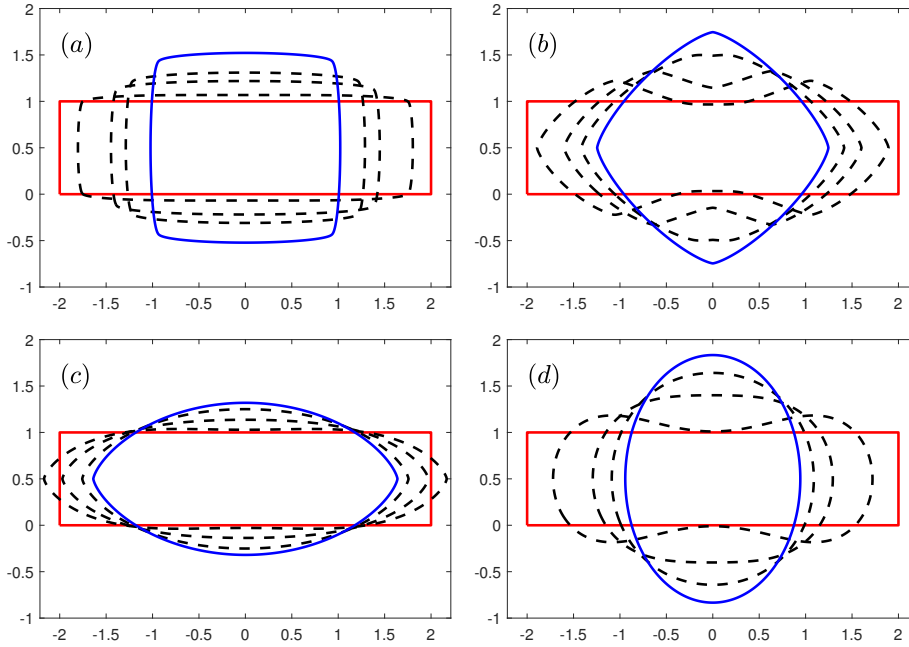


FIG. 5.4. Morphological evolutions of a close rectangular curve under anisotropic surface diffusion with different anisotropic surface energies: (a) regularized l^1 -norm metric $\gamma(\mathbf{n}) = \sqrt{n_1^2 + 0.01n_2^2} + \sqrt{0.01n_1^2 + n_2^2}$; (b) l^4 -norm metric $\gamma(\mathbf{n}) = \sqrt[4]{n_1^4 + n_2^4}$; (c) 2-fold $\gamma(\mathbf{n}) = 1 + \frac{1}{3} \cos(2(\theta - \frac{\pi}{2}))$; and (d) Riemannian-like metric $\gamma(\mathbf{n}) = \sqrt{\mathbf{n}^T \begin{pmatrix} 1 & 0 \\ 0 & 2 \end{pmatrix} \mathbf{n}}$, where the parameters $h = 2^{-6}, \tau = h^2$, and the red line, black dashed line, and blue line represent the initial shape, intermediate shape, and equilibrium shape, respectively.

Appendix A. The Cahn–Hoffman ξ -vector for several anisotropic surface energies. For the Riemannian-like metric surface energy (1.8), we have

$$(A.1) \quad \gamma(\mathbf{p}) = \sum_{l=1}^L \sqrt{\mathbf{p}^T \mathbf{G}_l \mathbf{p}} \quad \forall \mathbf{p} \in \mathbb{R}_*^2 := \mathbb{R}^2 \setminus \{\mathbf{0}\},$$

$$(A.2) \quad \boldsymbol{\xi} = \boldsymbol{\xi}(\mathbf{n}) = \sum_{l=1}^L \gamma_l(\mathbf{n})^{-1} \mathbf{G}_l \mathbf{n}, \quad \lambda(\mathbf{n}) = \sum_{l=1}^L \gamma_l(\mathbf{n})^{-3} \det(\mathbf{G}_l) > 0,$$

which indicates the Riemannian-like metric anisotropy is always weakly anisotropic.

For the l^r -norm ($r \geq 2$) metric anisotropic surface energy (1.9), we have

$$(A.3) \quad \gamma(\mathbf{p}) = \|\mathbf{p}\|_{l^r} = (|p_1|^r + |p_2|^r)^{\frac{1}{r}} \quad \forall \mathbf{p} = (p_1, p_2)^T \in \mathbb{R}_*^2,$$

$$(A.4) \quad \boldsymbol{\xi} = \boldsymbol{\xi}(\mathbf{n}) = \gamma(\mathbf{n})^{1-r} \begin{pmatrix} |n_1|^{r-2} n_1 \\ |n_2|^{r-2} n_2 \end{pmatrix}, \quad \lambda(\mathbf{n}) = (r-1) \frac{|n_1 n_2|^{r-2}}{\gamma(\mathbf{n})^{2r-1}}, \quad \forall \mathbf{n} \in \mathbb{S}^1,$$

which indicates the l^r -norm ($r \geq 2$) metric anisotropy is always weakly anisotropic.

For the m -fold anisotropic surface energy (1.10) with $\theta_0 = 0$, we have

$$(A.5) \quad \gamma(\mathbf{p}) = (p_1^2 + p_2^2)^{\frac{1}{2}} (1 + \beta \cos(m\theta)) \quad \forall \mathbf{p} = (p_1, p_2)^T = |p|(-\sin \theta, \cos \theta)^T \in \mathbb{R}_*^2.$$

Plugging (A.5) into (1.3), we get

$$(A.6) \quad \boldsymbol{\xi} = \boldsymbol{\xi}(\mathbf{n}) = \mathbf{n} + \beta \cos(m\theta) \mathbf{n} + \beta m \sin(m\theta) \mathbf{n}^\perp \quad \forall \mathbf{n} = (-\sin \theta, \cos \theta) \in \mathbb{S}^1,$$

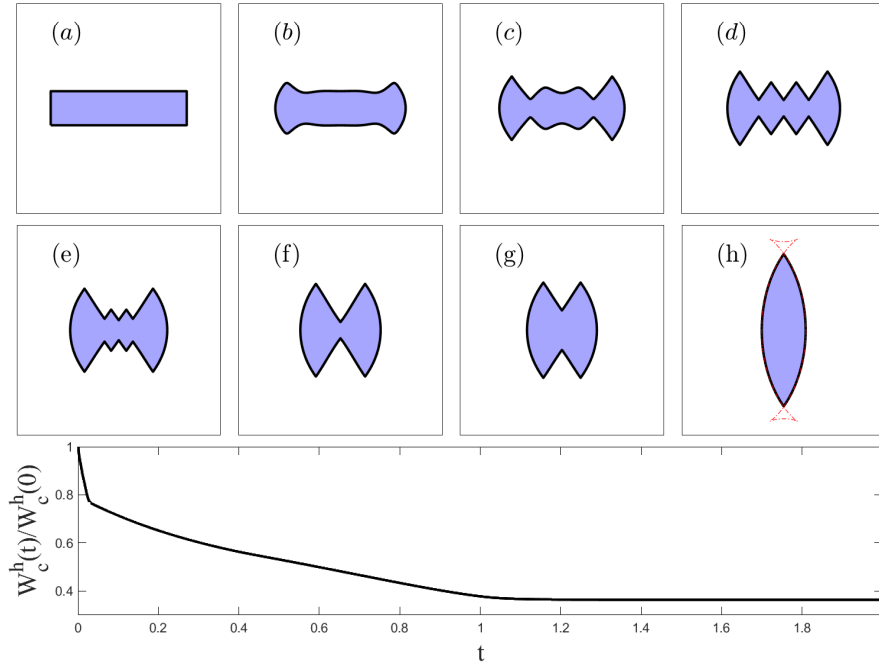


FIG. 5.5. Morphological evolutions and the normalized energy of a close rectangular curve under anisotropic surface diffusion with the strongly 2-fold anisotropic surface energy $\gamma(\mathbf{n}) = 1 + \frac{3}{5}\cos(2\theta)$ toward its equilibrium at different times: (a) $t = 0$, (b) $t = 10\tau$, (c) $t = 20\tau$, (d) $t = 100\tau$, (e) $t = 250\tau$, (f) $t = 500\tau$, (g) $t = 700\tau$, and (h) $t = 5000\tau$, where the other parameters are chosen the same as in Figure 5.4.

$$(A.7) \quad \lambda(\mathbf{n}) = 1 - \beta(m^2 - 1)\cos(m\theta),$$

which indicates that it is weakly anisotropic if $0 < \beta \leq \frac{1}{m^2 - 1}$; otherwise, it is strongly anisotropic.

For all the above $\gamma(\mathbf{n})$, their Hessian matrices are of the form

$$(A.8) \quad \mathbf{H}_\gamma(\mathbf{n}) = \lambda(\mathbf{n}) \begin{pmatrix} n_2^2 & -n_1 n_2 \\ -n_1 n_2 & n_1^2 \end{pmatrix} \quad \forall \mathbf{n} = (\mathbf{n}_1, \mathbf{n}_2)^T \in \mathbb{S}^1.$$

Appendix B. Proof of Lemma 4.7 for the Riemannian-like metric anisotropy.

Proof. First we consider the case $L = 1$ and assume $\mathbf{G}_1 = \begin{pmatrix} a & b \\ b & c \end{pmatrix} := \mathbf{G}$ with $a > 0$ and $ac - b^2 > 0$; then the minimal stabilizing function $k_0(\mathbf{n})$ becomes

$$(B.1) \quad k_0(\mathbf{n}) = \gamma(\mathbf{n})^{-1} \text{Tr}(\mathbf{G}) = \gamma(\mathbf{n})^{-1}(a + c) := k_1(\mathbf{n}).$$

By using ξ in (A.1), the corresponding surface energy matrix with respect to $k_1(\mathbf{n})$ can be given as

$$\begin{aligned} \mathbf{Z}_{k_1}(\mathbf{n}) &= \gamma(\mathbf{n})I_2 - \xi\mathbf{n}^T - \mathbf{n}\xi^T + k_1(\mathbf{n})\mathbf{nn}^T \\ &= \gamma(\mathbf{n})I_2 - \gamma(\mathbf{n})^{-1}\mathbf{G}\mathbf{nn}^T - \gamma(\mathbf{n})^{-1}\mathbf{nn}^T\mathbf{G} + \gamma(\mathbf{n})^{-1}(a + c)\mathbf{nn}^T \end{aligned}$$

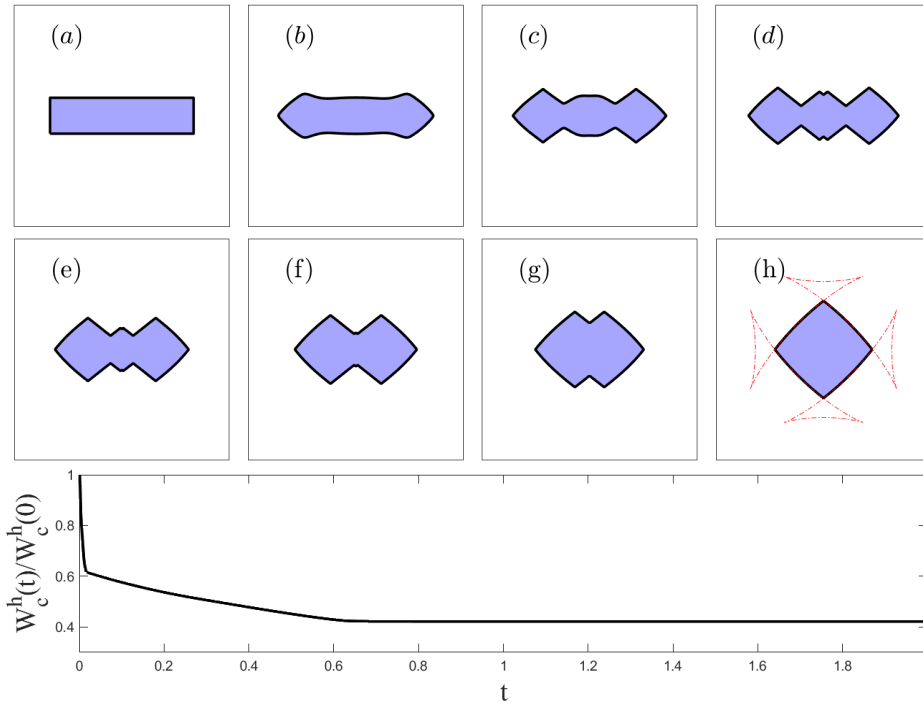


FIG. 5.6. Morphological evolutions and the normalized energy of a close rectangular curve under anisotropic surface diffusion with the strongly 4-fold anisotropic surface energy $\gamma(\mathbf{n}) = 1 + \frac{3}{10} \cos(4\theta)$ toward its equilibrium at different times: (a) $t = 0$, (b) $t = 5\tau$, (c) $t = 10\tau$, (d) $t = 20\tau$, (e) $t = 160\tau$, (f) $t = 300\tau$, (g) $t = 500\tau$, and (h) $t = 5000\tau$, where the parameters are chosen as $h = 2^{-5}$, $\tau = h^2$, and the red dashed line in (h) is the Wulff envelope.

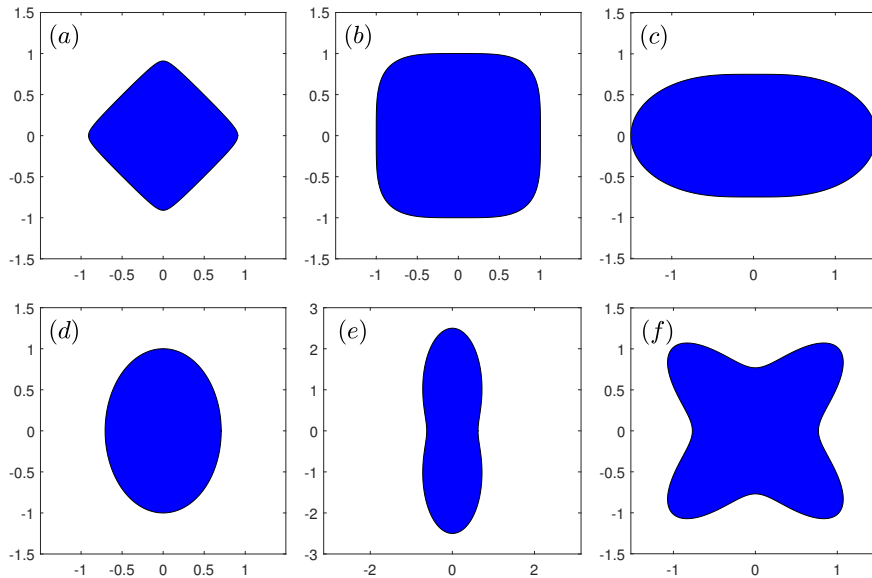


FIG. 5.7. The Frank diagrams of the weakly anisotropic energies: (a)–(d) used in Figure 5.4, respectively; and the strongly anisotropic energies: (e) $\gamma(\mathbf{n}) = 1 + \frac{3}{5} \cos(2\theta)$ in Figure 5.5, and (f) $\gamma(\mathbf{n}) = 1 + \frac{3}{10} \cos(4\theta)$ in Figure 5.6.

$$\begin{aligned}
&= \gamma(\mathbf{n})^{-1} \begin{pmatrix} \gamma(\mathbf{n})^2 - 2(an_1^2 + bn_1n_2) + (a+c)n_1^2 & * \\ -(an_1n_2 + bn_2^2) - (bn_1^2 + cn_1n_2) + (a+c)n_1n_2 & * \end{pmatrix} \\
\text{(B.2)} \quad &= \gamma(\mathbf{n})^{-1} \begin{pmatrix} c & -b \\ -b & a \end{pmatrix} = \gamma(\mathbf{n})^{-1} \mathbf{J}^T \mathbf{G} \mathbf{J},
\end{aligned}$$

where the * means the entry can be deduced in the same way. By direct computations, we obtain

$$\begin{aligned}
\gamma(\mathbf{n}) (\hat{\mathbf{n}}^\perp)^T \mathbf{Z}_{k_1}(\mathbf{n}) \hat{\mathbf{n}}^\perp - \gamma(\hat{\mathbf{n}})^2 &= (\hat{\mathbf{n}}^\perp)^T \mathbf{J}^T \mathbf{G} \mathbf{J} \hat{\mathbf{n}}^\perp - \gamma(\hat{\mathbf{n}})^2 \\
&= \hat{\mathbf{n}}^T \mathbf{G} \hat{\mathbf{n}} - \gamma(\hat{\mathbf{n}})^2 = 0.
\end{aligned}$$

From the alternative definition of $k_0(\mathbf{n})$ in (4.6), we obtain $k_0(\mathbf{n}) \leq k_1(\mathbf{n})$.

On the other hand, we take $\hat{\mathbf{n}} \rightarrow \mathbf{n}$ in $F(\mathbf{n}, \hat{\mathbf{n}})$. By applying (4.1) and the Hessian matrix derived in (A.1) and (A.8), we then have

$$\begin{aligned}
&(\mathbf{n}^\perp)^T \mathbf{H}_\gamma \mathbf{n}^\perp + \frac{|\boldsymbol{\xi}|^2}{\gamma(\mathbf{n})} \\
&= \gamma(\mathbf{n})^{-3} ((ac - b^2)(n_2^4 + 2n_1^2n_2^2 + n_1^4) + (an_1 + bn_2)^2 + (bn_1 + cn_2)^2) \\
&= \gamma(\mathbf{n})^{-3} (ac + a^2n_1^2 + 2abn_1n_2 + 2acn_1n_2 + c^2n_2^2) \\
&= \gamma(\mathbf{n})^{-3} (an_1^2 + 2bn_1n_2 + cn_2^2)(a + c) \\
&= \gamma(\mathbf{n})^{-1} (a + c) = k_0(\mathbf{n}),
\end{aligned}$$

which means $k_0(\mathbf{n}) \geq \gamma(\mathbf{n})^{-1}(a + c)$ by (3.13), hence $k_0(\mathbf{n}) = \gamma(\mathbf{n})^{-1} \text{Tr}(\mathbf{G}) = k_1(\mathbf{n})$.

For $L > 1$, Lemma 4.4 yields $k_1(\mathbf{n}) = \sum_{l=1}^L \gamma_l(\mathbf{n})^{-1} \text{Tr}(\mathbf{G}_l) \geq k_0(\mathbf{n})$, and $\mathbf{Z}_{k_1}(\mathbf{n})$ can be derived by the same argument in (B.2). \square

Appendix C. Proof of Lemma 4.8 for the l^r -norm metric anisotropy.

Proof. (i) When $r = 4$, a direct computation shows

$$\begin{aligned}
&\gamma(\mathbf{n}) (\hat{\mathbf{n}}^\perp)^T \mathbf{Z}_{k_0}(\mathbf{n}) \hat{\mathbf{n}}^\perp - \gamma(\hat{\mathbf{n}})^2 \\
&= \frac{1 - 2n_1n_2\hat{n}_1\hat{n}_2}{\sqrt{n_1^4 + n_2^4}} - \sqrt{\hat{n}_1^4 + \hat{n}_2^4} \\
&= \frac{(n_1^2 + n_2^2)^2 + (\hat{n}_1^2 + \hat{n}_2^2)^2 - 4n_1n_2\hat{n}_1\hat{n}_2 - 2\sqrt{\hat{n}_1^4 + \hat{n}_2^4}\sqrt{n_1^4 + n_2^4}}{2\sqrt{n_1^4 + n_2^4}} \\
&\geq \frac{(n_1^2 + n_2^2)^2 + (\hat{n}_1^2 + \hat{n}_2^2)^2 - 4n_1n_2\hat{n}_1\hat{n}_2 - n_1^4 - n_2^4 - \hat{n}_1^4 - \hat{n}_2^4}{2\sqrt{n_1^4 + n_2^4}} \\
&= \frac{(n_1n_2 - \hat{n}_1\hat{n}_2)^2}{\sqrt{n_1^4 + n_2^4}} \geq 0 \quad \forall \mathbf{n}, \hat{\mathbf{n}} \in \mathbb{S}^1.
\end{aligned}$$

By Theorem 4.2, we get $k_0(\mathbf{n}) \leq 2\gamma(\mathbf{n})^{-3}$. On the other hand, by taking $\hat{\mathbf{n}} = (n_2, n_1)^T \in \mathbb{S}^1$ in (3.12) and the $\boldsymbol{\xi}$ vector given in (A.4), we obtain

$$\begin{aligned}
F(\mathbf{n}, \hat{\mathbf{n}}) &= \frac{2\gamma(\mathbf{n})(\gamma(\mathbf{n})^{-3}(n_1^3, n_2^3) \cdot (-n_1, n_2))(-n_1^2 + n_2^2)}{\gamma(\mathbf{n})(-n_1^2 + n_2^2)^2} \\
&= 2\gamma(\mathbf{n})^{-3} \frac{(-n_1^2 + n_2^2)^2(n_2^2 + n_1^2)}{(-n_1^2 + n_2^2)^2} = 2\gamma(\mathbf{n})^{-3}.
\end{aligned}$$

By (3.13), we know that $k_0(\mathbf{n}) \geq 2\gamma(\mathbf{n})^{-3}$, hence $k_0(\mathbf{n}) = 2\gamma(\mathbf{n})^{-3}$.

(ii) When $r = 6$, a direct computation shows

$$\begin{aligned} & \gamma(\mathbf{n}) (\hat{\mathbf{n}}^\perp)^T Z_{k_0}(\mathbf{n}) \hat{\mathbf{n}}^\perp - \gamma(\hat{\mathbf{n}})^2 \\ &= \gamma(\mathbf{n})^{-4} (1 - n_1^2 n_2^2 - 2n_1 n_2 \hat{n}_1 \hat{n}_2) - \sqrt[3]{\hat{n}_1^6 + \hat{n}_2^6} \\ &= \gamma(\mathbf{n})^{-4} \left(1 - n_1^2 n_2^2 - 2n_1 n_2 \hat{n}_1 \hat{n}_2 - \sqrt[3]{(n_1^6 + n_2^6)^2 (\hat{n}_1^6 + \hat{n}_2^6)} \right) \\ &\geq \gamma(\mathbf{n})^{-4} \left(\frac{2(n_1^2 + n_2^2)^3 + (\hat{n}_1^2 + \hat{n}_2^2)^3}{3} - n_1^2 n_2^2 - 2n_1 n_2 \hat{n}_1 \hat{n}_2 - \frac{2(n_1^6 + n_2^6) + (\hat{n}_1^6 + \hat{n}_2^6)}{3} \right) \\ &= \gamma(\mathbf{n})^{-4} \left(\frac{6n_1^4 n_2^2 + 6n_1^2 n_2^4 + 3\hat{n}_1^4 \hat{n}_2^2 + 3\hat{n}_1^2 \hat{n}_2^4}{3} - n_1^2 n_2^2 - 2n_1 n_2 \hat{n}_1 \hat{n}_2 \right) \\ &= \gamma(\mathbf{n})^{-4} (2n_1^2 n_2^2 (n_1^2 + n_2^2) + \hat{n}_1^2 \hat{n}_2^2 (\hat{n}_1^2 + \hat{n}_2^2) - n_1^2 n_2^2 - 2n_1 n_2 \hat{n}_1 \hat{n}_2) \\ &= \gamma(\mathbf{n})^{-4} (n_1 n_2 - \hat{n}_1 \hat{n}_2)^2 \geq 0 \quad \forall \mathbf{n}, \hat{\mathbf{n}} \in \mathbb{S}^1. \end{aligned}$$

By Theorem 4.2, we get $k_0(\mathbf{n}) \leq 2\gamma(\mathbf{n})^{-5}(n_2^4 + n_2^2 n_1^2 + n_1^4)$. On the other hand, by taking $\hat{\mathbf{n}} = (n_2, n_1)^T \in \mathbb{S}^1$ in (3.12) and the $\boldsymbol{\xi}$ vector given in (A.4), we obtain

$$\begin{aligned} F(\mathbf{n}, \hat{\mathbf{n}}) &= \frac{2\gamma(\mathbf{n})(\gamma(\mathbf{n})^{-5}(n_1^5, n_2^5) \cdot (-n_1, n_2))(-n_1^2 + n_2^2)}{\gamma(\mathbf{n})(-n_1^2 + n_2^2)^2} \\ &= 2\gamma(\mathbf{n})^{-5} \frac{(-n_1^2 + n_2^2)^2 (n_2^4 + n_2^2 n_1^2 + n_1^4)}{(-n_1^2 + n_2^2)^2} = 2\gamma(\mathbf{n})^{-5} (n_2^4 + n_2^2 n_1^2 + n_1^4). \end{aligned}$$

By (3.13), we know that $k_0(\mathbf{n}) \geq 2\gamma(\mathbf{n})^{-5}(n_2^4 + n_2^2 n_1^2 + n_1^4)$, hence $k_0(\mathbf{n}) = 2\gamma(\mathbf{n})^{-5}(n_2^4 + n_2^2 n_1^2 + n_1^4)$. \square

Appendix D. Proof of Lemma 4.9 for the 2/4-fold anisotropy.

Proof. For the m -fold anisotropy $\hat{\gamma}(\theta) = \gamma(\mathbf{n}) = 1 + \beta \cos m\theta$, we know that $\hat{\gamma}'(\theta) = -m\beta \sin m\theta$. The $\tilde{F}^\theta(\hat{\theta})$ given in (4.14) is

$$\begin{aligned} \tilde{F}^\theta(\hat{\theta}) &= 2(1 + \beta \cos m\theta) \\ &+ \frac{(1 + \beta \cos m\hat{\theta})^2 - (1 + \beta \cos m\theta)^2}{(1 + \beta \cos m\theta) \sin^2(\hat{\theta} - \theta)} + \frac{m\beta \sin m\theta \sin(2(\hat{\theta} - \theta))}{\sin^2(\hat{\theta} - \theta)}. \end{aligned} \tag{D.1}$$

(i) For the 2-fold anisotropy, i.e., $m = 2$, by applying Mathematica to (D.1), we get

$$\tilde{F}^\theta(\hat{\theta}) = 4 - 2(1 + \beta \cos 2\theta) + \frac{2\beta^2(1 - \cos 2(\hat{\theta} + \theta))}{1 + \beta \cos 2\theta}. \tag{D.2}$$

Thus by (4.13) in Remark 4.1, we obtain

$$k_0(\mathbf{n}) = \max_{\hat{\theta} \in [\theta - \frac{\pi}{2}, \theta + \frac{\pi}{2}]} \tilde{F}^\theta(\hat{\theta}) \leq 4 - 2\gamma(\mathbf{n}) + \frac{4\beta^2}{\gamma(\mathbf{n})}. \tag{D.3}$$

On the other hand, by taking $\hat{\theta} = \frac{\pi}{2} - \theta$ in (D.2), we obtain

$$\tilde{F}^\theta\left(\frac{\pi}{2} - \theta\right) = 4 - 2\gamma(\mathbf{n}) + \frac{4\beta^2}{\gamma(\mathbf{n})} \leq k_0(\mathbf{n}). \tag{D.4}$$

By combining (D.3) and (D.4), we know $k_0(\mathbf{n}) = 4 - 2\gamma(\mathbf{n}) + \frac{4\beta^2}{\gamma(\mathbf{n})}$, which validates (4.25).

Downloaded 04/06/23 to 137.132.123.69 . Redistribution subject to SIAM license or copyright; see https://pubs.siam.org/terms-privacy

(ii) For the 4-fold anisotropy, i.e., $m = 4$, by applying Mathematica to (D.1), we get

$$(D.5) \quad \begin{aligned} \tilde{F}^\theta(\hat{\theta}) = & 2\gamma(\mathbf{n}) - \frac{16\beta \cos(\hat{\theta} - \theta) \cos(\hat{\theta} + 3\theta)}{\gamma(\mathbf{n})} \\ & - \frac{4\beta^2 \cos(\hat{\theta} - \theta)(2 \cos(\hat{\theta} + 7\theta) + \cos(3\hat{\theta} + 5\theta) + \cos(5\hat{\theta} + 3\theta))}{\gamma(\mathbf{n})}. \end{aligned}$$

Thus by (4.13) in Remark 4.1, we obtain

$$(D.6) \quad k_0(\mathbf{n}) = \max_{\hat{\theta} \in [\theta - \frac{\pi}{2}, \theta + \frac{\pi}{2}]} \tilde{F}^\theta(\hat{\theta}) \leq 2\gamma(\mathbf{n}) + \frac{16\beta + 16\beta^2}{\gamma(\mathbf{n})} = k_1(\mathbf{n}),$$

which validates (4.26). \square

REFERENCES

- [1] E. BÄNSCH, P. MORIN, AND R. H. NOCHETTO, *Surface diffusion of graphs: Variational formulation, error analysis, and simulation*, SIAM J. Numer. Anal., 42 (2004), pp. 773–799.
- [2] W. BAO, H. GARCKE, R. NÜRNBERG, AND Q. ZHAO, *Volume-preserving parametric finite element methods for axisymmetric geometric evolution equations*, J. Comput. Phys., 460 (2022), 111180.
- [3] W. BAO, W. JIANG, D. J. SROLOVITZ, AND Y. WANG, *Stable equilibria of anisotropic particles on substrates: A generalized winterbottom construction*, SIAM J. Appl. Math., 77 (2017), pp. 2093–2118.
- [4] W. BAO, W. JIANG, Y. WANG, AND Q. ZHAO, *A parametric finite element method for solid-state dewetting problems with anisotropic surface energies*, J. Comput. Phys., 330 (2017), pp. 380–400.
- [5] W. BAO AND Q. ZHAO, *A structure-preserving parametric finite element method for surface diffusion*, SIAM J. Numer. Anal., 59 (2021), pp. 2775–2799.
- [6] J. W. BARRETT, H. GARCKE, AND R. NÜRNBERG, *A parametric finite element method for fourth order geometric evolution equations*, J. Comput. Phys., 222 (2007), pp. 441–467.
- [7] J. W. BARRETT, H. GARCKE, AND R. NÜRNBERG, *Numerical approximation of anisotropic geometric evolution equations in the plane*, IMA J. Numer. Anal., 28 (2008), pp. 292–330.
- [8] J. W. BARRETT, H. GARCKE, AND R. NÜRNBERG, *A variational formulation of anisotropic geometric evolution equations in higher dimensions*, Numer. Math., 109 (2008), pp. 1–44.
- [9] J. W. BARRETT, H. GARCKE, AND R. NÜRNBERG, *The approximation of planar curve evolutions by stable fully implicit finite element schemes that equidistribute*, Numer. Methods Partial Differential Equations, 27 (2011), pp. 1–30.
- [10] J. W. BARRETT, H. GARCKE, AND R. NÜRNBERG, *Parametric finite element approximations of curvature-driven interface evolutions*, in Geometric Partial Differential Equations - Part I, Handb. Numer. Anal. 21, Elsevier, Amsterdam, 2020, pp. 275–423.
- [11] J. CAHN, *Stability, microstructural evolution, grain growth, and coarsening in a two-dimensional two-phase microstructure*, Acta Metall. Mater., 39 (1991), pp. 2189–2199.
- [12] J. W. CAHN AND J. E. TAYLOR, *Surface motion by surface diffusion*, Acta Metall. Mater., 42 (1994), pp. 1045–1063.
- [13] U. CLARENZ, U. DIEWALD, AND M. RUMPF, *Anisotropic geometric diffusion in surface processing*, in Proceedings of Visualization 2000, IEEE, 2000.
- [14] K. DECKELNICK, G. DZIUK, AND C. M. ELLIOTT, *Computation of geometric partial differential equations and mean curvature flow*, Acta Numer., 14 (2005), pp. 139–232.
- [15] K. DECKELNICK, G. DZIUK, AND C. M. ELLIOTT, *Fully discrete finite element approximation for anisotropic surface diffusion of graphs*, SIAM J. Numer. Anal., 43 (2005), pp. 1112–1138.
- [16] P. DU, M. KHENNER, AND H. WONG, *A tangent-plane marker-particle method for the computation of three-dimensional solid surfaces evolving by surface diffusion on a substrate*, J. Comput. Phys., 229 (2010), pp. 813–827.
- [17] I. FONSECA, A. PRATELLI, AND B. ZWICKNAGL, *Shapes of epitaxially grown quantum dots*, Arch. Ration. Mech. Anal., 214 (2014), pp. 359–401.
- [18] F. HAUSSER AND A. VOIGT, *A discrete scheme for regularized anisotropic surface diffusion: A 6th order geometric evolution equation*, Interfaces Free Bound., 7 (2005), pp. 353–370.
- [19] F. HAUSSER AND A. VOIGT, *A discrete scheme for parametric anisotropic surface diffusion*, J. Sci. Comput., 30 (2007), pp. 223–235.

- [20] D. W. HOFFMAN AND J. W. CAHN, *A vector thermodynamics for anisotropic surfaces: I. Fundamentals and application to plane surface junctions*, Surf. Sci., 31 (1972), pp. 368–388.
- [21] W. HUANG, W. JIANG, AND Q. ZHAO, *A $\theta - L$ formulation-based finite element method for solving axisymmetric solid-state dewetting problems*, East Asian J. Appl. Math., 11 (2021), pp. 389–405.
- [22] W. JIANG, W. BAO, C. V. THOMPSON, AND D. J. SROLOVITZ, *Phase field approach for simulating solid-state dewetting problems*, Acta Mater., 60 (2012), pp. 5578–5592.
- [23] W. JIANG AND B. LI, *A perimeter-decreasing and area-conserving algorithm for surface diffusion flow of curves*, J. Comput. Phys., 443 (2021), 110531.
- [24] W. JIANG, Y. WANG, Q. ZHAO, D. J. SROLOVITZ, AND W. BAO, *Solid-state dewetting and island morphologies in strongly anisotropic materials*, Scr. Mater., 115 (2016), pp. 123–127.
- [25] W. JIANG AND Q. ZHAO, *Sharp-interface approach for simulating solid-state dewetting in two dimensions: A Cahn–Hoffman ξ -vector formulation*, Phys. D, 390 (2019), pp. 69–83.
- [26] W. JIANG, Q. ZHAO, AND W. BAO, *Sharp-interface model for simulating solid-state dewetting in three dimensions*, SIAM J. Appl. Math., 80 (2020), pp. 1654–1677.
- [27] B. KOVÁCS, B. LI, AND C. LUBICH, *A convergent evolving finite element algorithm for willmore flow of closed surfaces*, Numer. Math., 149 (2021), pp. 595–643.
- [28] B. LI, J. LOWENGRUB, A. RATZ, AND A. VOIGT, *Geometric evolution laws for thin crystalline films: Modeling and numerics*, Commun. Comput. Phys., 6 (2009), pp. 433–482.
- [29] Y. LI AND W. BAO, *An energy-stable parametric finite element method for anisotropic surface diffusion*, J. Comput. Phys., 446 (2021), 110658.
- [30] Z. LI, H. ZHAO, AND H. GAO, *A numerical study of electro-migration voiding by evolving level set functions on a fixed cartesian grid*, J. Comput. Phys., 152 (1999), pp. 281–304.
- [31] U. F. MAYER, *Numerical solutions for the surface diffusion flow in three space dimensions*, Comput. Appl. Math., 20 (2001), pp. 361–379.
- [32] W. W. MULLINS, *Theory of thermal grooving*, J. Appl. Phys., 28 (1957), pp. 333–339.
- [33] B. J. SPENCER, *Asymptotic solutions for the equilibrium crystal shape with small corner energy regularization*, Phys. Rev. E, 69 (2004), 011603.
- [34] A. P. SUTTON AND R. W. BALLUFFI, *Interfaces in Crystalline Materials*, Clarendon Press, Oxford, UK, 1995.
- [35] J. E. TAYLOR, *Mean curvature and weighted mean curvature*, Acta Metall. Mater., 40 (1992), pp. 1475–1485.
- [36] J. E. TAYLOR AND J. W. CAHN, *Linking anisotropic sharp and diffuse surface motion laws via gradient flows*, J. Stat. Phys., 77 (1994), pp. 183–197.
- [37] C. V. THOMPSON, *Solid-state dewetting of thin films*, Annu. Rev. Mater. Res., 42 (2012), pp. 399–434.
- [38] S. TORABI, J. LOWENGRUB, A. VOIGT, AND S. WISE, *A new phase-field model for strongly anisotropic systems*, Proc. A, 465 (2009), pp. 1337–1359.
- [39] Y. WANG, W. JIANG, W. BAO, AND D. J. SROLOVITZ, *Sharp interface model for solid-state dewetting problems with weakly anisotropic surface energies*, Phys. Rev. B, 91 (2015), 045303.
- [40] A. WHEELER, *Cahn–Hoffman ξ -vector and its relation to diffuse interface models of phase transitions*, J. Stat. Phys., 95 (1999), pp. 1245–1280.
- [41] H. WONG, P. VOORHEES, M. MIKSI, AND S. DAVIS, *Periodic mass shedding of a retracting solid film step*, Acta Mater., 48 (2000), pp. 1719–1728.
- [42] G. WULFF, *Zur frage der geschwindigkeit des wachstums und der auflösung der krystallflächen*, Z. Kristallogr., 34 (1901), pp. 449–530.
- [43] L. XIA, A. F. BOWER, Z. SUO, AND C. SHIH, *A finite element analysis of the motion and evolution of voids due to strain and electromigration induced surface diffusion*, J. Mech. Phys. Solids, 45 (1997), pp. 1473–1493.
- [44] Y. XU AND C.-W. SHU, *Local discontinuous Galerkin method for surface diffusion and Willmore flow of graphs*, J. Sci. Comput., 40 (2009), pp. 375–390.
- [45] J. YE AND C. V. THOMPSON, *Mechanisms of complex morphological evolution during solid-state dewetting of single-crystal nickel thin films*, Appl. Phys. Lett., 97 (2010), 071904.
- [46] Q. ZHAO, W. JIANG, AND W. BAO, *A parametric finite element method for solid-state dewetting problems in three dimensions*, SIAM J. Sci. Comput., 42 (2020), pp. B327–B352.
- [47] Q. ZHAO, W. JIANG, AND W. BAO, *An energy-stable parametric finite element method for simulating solid-state dewetting*, IMA J. Numer. Anal., 41 (2021), pp. 2026–2055.